Secreted ADAMTS-like 2 promotes myoblast differentiation by potentiating Wnt signaling

Taye Nandaraj[1], **Singh Mukti**[2], **Baldock Clair**[2], **Hubmacher Dirk**[1]

[1]Orthopedic Research Laboratories, Leni & Peter W. May Department of Orthopedics, Icahn School of Medicine at Mount Sinai, New York, NY, 10029, USA.

[2]Division of Cell-Matrix Biology and Regenerative Medicine, School of Biological Sciences, Faculty of Biology, Medicine and Health, Wellcome Centre for Cell-Matrix Research, Manchester Academic Health Science Centre, University of Manchester, Manchester, UK

Abstract

Myogenesis is the process that generates multinucleated contractile myofibers from muscle stem cells during skeletal muscle development and regeneration. Myogenesis is governed by myogenic regulatory transcription factors, including MYOD1. Here, we identified the secreted matricellular protein ADAMTS-like 2 (ADAMTSL2) as part of a Wnt-dependent positive feedback loop which augmented or sustained MYOD1 expression and thus promoted myoblast differentiation. ADAMTSL2 depletion resulted in severe retardation of myoblast differentiation in vitro and its ablation in myogenic precursor cells resulted in aberrant skeletal muscle architecture. Mechanistically, ADAMTSL2 potentiated WNT signaling by binding to WNT ligands and WNT receptors. We identified the WNT-binding ADAMTSL2 peptide, which was sufficient to promote myogenesis in vitro. Since ADAMTSL2 was previously described as a negative regulator of TGFβ signaling in fibroblasts, ADAMTSL2 now emerges as a signaling hub that could integrate WNT, TGFβ and potentially other signaling pathways within the dynamic microenvironment of differentiating myoblasts during skeletal muscle development and regeneration.

Keywords

extracellular matrix; acromelic dysplasia; ADAMTS proteases; ADAMTSL proteins; skeletal muscle

Introduction

Skeletal muscles account for up to 40% of total body weight and are required for locomotion, respiration, feeding, and communication [1]. Skeletal muscles are powered by the reversible contraction of multinucleated myofibers, which are formed during embryonic and postnatal development in a process called myogenesis. During myogenesis, myogenic precursor cells (muscle stem cells) differentiate into proliferating myoblasts, which exit the cell cycle and become myocytes [2]. Myocytes then fuse with each other to form multinucleated myofibers. Myogenesis is governed by the sequential expression of the myogenic regulatory transcription factors MYF5, MYOD1, MYOG, and MRF4 [3]. MYOD-deficiency resulted in increased myoblast proliferation and compromised myogenic differentiation [4–6]. MYOD can be induced by WNT and other signaling pathways [7–10]. During early development, canonical WNT signaling is required for dermomyotome function and myofiber specification [11, 12]. Non-canonical WNT signaling can also induce MYOD expression and regulate myocyte elongation [13, 14]. Thus, the balance between canonical and non-canonical WNT signaling and integration of WNT signaling with other signaling pathways may ultimately regulate myogenesis and fine-tune skeletal muscle development.

Matricellular proteins are regulatory extracellular matrix (ECM) proteins that control signaling pathways, including WNT and TGFβ signaling, where they act as rheostats by conferring latency to signaling molecules or potentiating their signaling capacity, by establishing growth factor gradients, or by regulating growth factor-receptor interactions [15–18]. The matricellular protein ADAMTS-like 2 (ADAMTSL2), which shares homology with ADAMTS proteases but lacks their protease domain, was identified as a negative regulator of TGFβ signaling in bronchial smooth muscle cells, chondrocytes, and skin and cardiac fibroblasts [19–23]. In humans, pathogenic variants in *ADAMTSL2* cause geleophysic dysplasia (GD), which is characterized by short stature, joint stiffness, pseudomuscularity, tight skin, and life-threatening heart valve and airway anomalies [22, 24]. *ADAMTSL2* variants have also been linked to neonatal lethal Al-Gazali skeletal dysplasia and an autosomal dominant disorder with features of dermatosparaxic Ehlers-Danlos syndrome [25, 26].

Here, we used in vitro and in vivo gain- and loss-of-function studies to interrogate the role of ADAMTSL2 in skeletal muscle development and identified an unexpected role for ADAMTSL2 as a positive regulator of myogenesis. ADAMTSL2 was expressed during myoblast differentiation downstream of MYOD and its knockdown or overexpression abolished or promoted myoblast to myotube differentiation, respectively, indicating an essential role in myogenesis. Mechanistically, ADAMTSL2 potentiated WNT signaling by binding to multiple WNT ligands and the canonical WNT co-receptor LRP6, suggesting that ADAMTSL2 may increase the signaling potency of endogenous WNT ligands during muscle differentiation. Conditional deletion of *Adamtsl2* in MYF5-positive myogenic progenitor cells resulted in increased muscle weight, mimicking muscle manifestations in patients with GD. Collectively, these findings identify ADAMTSL2 as a novel rheostat for WNT signaling and a critical regulator of myogenesis, where ADAMTSL2 participates in a WNT ligand-dependent positive feedback loop that augments MYOD expression.

Results

ADAMTSL2 is required for myoblast differentiation

To investigate the function of ADAMTSL2 during myogenesis, we used the emergence of multinucleated myosin heavy chain (MyHC)-positive myotubes following myoblast differentiation induced by serum-reduction as assay (Fig. 1A). To validate a previous report showing induction of *Adamtsl2* expression in differentiating myoblasts, we measured *Adamtsl2* mRNA levels in differentiating C2C12 myoblasts (Fig. 1B) [23]. C2C12 myoblasts significantly upregulated ADAMTSL2 mRNA levels after induction of differentiation with a peak at 2 days and sustained levels until day 7. Notably, increased ADAMTSL2 mRNA expression preceded MYH4 (MyHC) induction and myotube formation. On the protein level, ADAMTSL2 was detected in MyHC-positive myocytes and multinucleated myotubes (Fig 1C, D). We next quantified *Adamtsl2* expression in differentiating primary wild-type mouse myoblasts isolated from extensor digitorum longus (EDL) muscles (Fig. 1E–G). ADAMTSL2 mRNA levels were upregulated at 1 day and peaked at 2 days after induction of differentiation (Fig. 1E). ADAMTSL2 protein levels strongly increased at 3 days post differentiation induction and localized to MyHC-positive myocytes and myotubes similar to differentiating C2C12 myoblasts (Fig. 1F, G) [27]. Finally, we measured ADAMTSL2 mRNA levels in differentiating primary human myoblasts (Fig. 1H). We observed a biphasic expression pattern with strong ADAMTSL2 mRNA induction at 1 and 5 days after differentiation initiation (Fig. 1H). MYH4 expression increased gradually indicating myoblast differentiation. ADAMTSL2 protein localized to MyHC-positive human myocytes and myotubes though less myotubes were observed at 3 days after differentiation initiation (Fig. 1I, J).

To identify the function of ADAMTSL2 during myoblast differentiation, we depleted ADAMTSL2 mRNA in C2C12 myoblasts by stable expression of an ADAMTSL2-targeting shRNA (*Adamtsl2*-KD), which significantly reduced ADAMTSL2 mRNA and protein levels compared to control shRNA (sh-Ctrl) (Fig. 2A, B). Strikingly, *Adamtsl2*-KD myoblasts failed to differentiate as indicated by the absence of MyHC-positive myocytes or myotubes (Fig. 2C, middle). As a result, the fusion index, i.e. the percentage of nuclei within multinucleated MyHC-positive myotubes, was significantly reduced (Fig. 2D). Lack of differentiation of *Adamtsl2*-KD myoblasts was fully rescued by transient overexpression of full-length ADAMTSL2 (p*ADAMTSL2*) (Fig. 2C, right). Importantly, the fusion index after ADAMTSL2 overexpression was not only normalized but was increased ~1.6-fold compared to sh-Ctrl conditions (Fig. 2D). Consistent with this observation, differentiation of C2C12 myoblasts that constitutively overexpressed full-length ADAMTSL2 resulted in larger myotubes and the fusion index was increased ~1.8-fold after 5 days of differentiation (Fig. 2E, F). When ADAMTSL2 was transiently overexpressed in primary human myoblasts, the fusion index was increased by ~3-fold at 5 days after differentiation initiation (Fig. 2G, H). Finally, addition of recombinant ADAMTSL2 protein (rADAMTSL2) to C2C12 myoblasts augmented myotube formation in a dose dependent manner (Fig. 2I–K).

Collectively, our data demonstrate that ADAMTSL2 expression is strongly induced during the differentiation of mouse and human myoblasts and that ADAMTSL2 promotes myogenesis.

ADAMTSL2 is a MYOD target gene and participates in a positive feedback loop

To identify molecular pathways that could explain the lack of differentiation of *Adamtsl2*-deficient myoblasts, we determined differentially expressed genes (DEGs) between *Adamtsl2*-KD and sh-Ctrl C2C12 myoblasts 3 days after initiation of differentiation by RNA sequencing (RNAseq). Consistent with a lack of differentiation, we observed downregulation of myogenic transcription factors (*Pax7*, *Myod1*, *Mrf4*, *Myog*), MyHC (*Myh4*) and of genes required for myocyte fusion (*Mymk*, *Mymx*), which we confirmed in an independent sample set (Fig. 3A, B). The same genes were upregulated when ADAMTSL2 was overexpressed in C2C12 myoblasts (Fig. 3C). Since myoblast differentiation requires cell cycle exit and cessation of cell proliferation, we measured proliferation using Ki67 immunostaining. Myoblast proliferation was significantly increased in *Adamtsl2*-KD cells and decreased in ADAMTSL2-overexpressing cells, consistent with lack or promotion of myoblast differentiation, respectively (Fig. 3D–G). Proliferation of primary human myoblasts was also reduced after transient overexpression of ADAMTSL2, although proliferation at baseline was 3–4-fold lower compared to C2C12 myoblasts (Fig. 3H, I).

Since the *Adamtsl2*-KD phenotype is reminiscent of increased proliferation and lack of differentiation observed in MYOD-deficient myoblasts, we cross-referenced DEGs from *Adamtsl2*-KD C2C12 myoblasts with published DEGs from *Myod1* knockout (*Myod1*-KO) C2C12 myoblasts, both under differentiation conditions [28]. A Venn diagram shows that 19.4% (n = 1,113/5,720) of *Adamtsl2*-KD DEGs were shared with *Myod1*-KO DEGs (Fig. 3J). Consistent with lack of myoblast differentiation in both cell lines, shared DEGs were almost exclusively enriched in gene sets related to skeletal muscle, myotube formation or myoblast differentiation (Fig. 3K). Interestingly, *Myod1*-KO specific DEGs (n = 1,419/2,602) were enriched in neurotransmission, neuron projection arborization, immune interactions, and ECM organization (Fig. 3L). In contrast, *Adamtsl2*-KD specific DEGs (n = 4,607/5,720) enrichment suggested involvement in regulation of bone and fat cell differentiation and growth factor signaling including WNT and BMP (Fig. 3M). Molecular Signature Database (MSigDB) analysis showed a much higher combined score for the enrichment of myogenesis-related genes in the shared and *Adamtsl2*-KD-specific DEGs compared to *Myod1*-KO-specific DEGs (Fig. 3N). These analyses raised the possibility of a relationship between MYOD and ADAMTSL2. Therefore, we first analyzed the mouse and human ADAMTSL2 promoter sequence and identified 13 and 10 putative MYOD binding sites, respectively, in the 2 kb region upstream of the transcriptional start site suggesting direct regulation of ADAMTSL2 by MYOD (Fig. 3O). Next, we knocked down MYOD using *Myod1*-directed shRNA (*Myod1*-KD) and measured ADAMTSL2 mRNA levels (Fig. 3P). *Myod1*-KD resulted in ~80% reduction of MYOD mRNA expression and a concomitant significant reduction of ADAMTSL2 mRNA suggesting a direct regulation of *Adamtsl2* by MYOD, while overexpression of ADAMTSL2 resulted in increased MYOD expression. Strikingly, ADAMTSL2 induced MYOD mRNA levels in a WNT-dependent

manner (see below), since inhibition of WNT ligand secretion with the porcupine inhibitor LGK 974 reduced MYOD mRNA levels back to baseline, even when ADAMTSL2 was overexpressed (Fig. 3Q) [29]. To determine, if ADAMTSL2 could independently rescue MYOD-deficiency in C2C12 cells, we transfected ADAMTSL2 in *MyoD1*-KD C2C12 myoblasts after establishing sh-*MyoD1* expression and stained for MyHC-positive myotubes (Fig. 3R, S). Overexpression of ADAMTSL2 promoted myogenesis as shown above, but was unable to overcome MYOD-deficiency (Fig. 3R, S). Together, these data suggest that ADAMTSL2 is a critical component of the MYOD-regulated myoblast differentiation program, where it may participate in a WNT-dependent positive feedback loop to augment or sustain MYOD expression.

ADAMTSL2 regulates canonical WNT signaling

To determine how ADAMTSL2 regulates myoblast differentiation downstream of MYOD, we first considered regulation of TGFβ signaling, since elevated TGFβ signaling due to ADAMTSL2 depletion would be consistent with reduced myoblast differentiation [30, 31]. However, SMAD2/3 phosphorylation, a readout for canonical TGFβ signaling, was not changed in *Adamtsl2*-KD myoblasts, suggesting TGFβ-independent effects on myoblast differentiation (Fig. 4A). Next, we considered disruption of WNT signaling in *Adamtsl2*-KD myoblasts since DEGs associated with WNT/β-catenin signaling were enriched in shared and *Adamtsl2*-KD-specific DEGs, and WNT signaling is required for myoblast differentiation [9, 10, 32, 33]. We used β-catenin stabilization and its nuclear translocation as readouts for canonical WNT/β-catenin signaling (Fig. 4B). Total β-catenin levels, as determined by western blotting, were reduced in differentiating *Adamtsl2*-KD myoblasts and increased when ADAMTSL2 was overexpressed or added as recombinant protein to C2C12 and primary human myoblasts, suggesting that ADAMTSL2 potentiates WNT/β-catenin signaling (Fig. 4C–F). Lithium chloride (LiCl), which activates canonical WNT signaling, was used as positive control [34]. Consistent with positive regulation of WNT signaling, β-catenin levels visualized by immunofluorescence microscopy were reduced in *Adamtsl2*-KD myoblasts and no nuclear localization was observed (Fig. 4G, middle row). In contrast, ADAMTSL2 overexpression resulted in the almost exclusive localization of β-catenin in the nucleus (Fig. 4G, bottom row). To correlate temporal regulation of ADAMTSL2, β-catenin and MyHC during myoblast differentiation, we analyzed cell lysates from a time course of differentiating myoblasts by western blotting (Fig. 4H–J). Consistent with ADAMTSL2 mRNA kinetics, ADAMTSL2 in C2C12 myoblasts peaked at day 2 after differentiation initiation correlating with a peak in β-catenin and followed by induction of MyHC (Fig. 4H). In lysates from *Adamtsl2*-KD myoblasts, ADAMTSL2 protein was significantly reduced and unchanged during myoblast differentiation (Fig. 4I). Concomitantly, cellular β-catenin levels not associated with WNT signaling remained constant at a low level and MyHC was not induced. A similar correlation of ADAMTSL2, β-catenin, and MyHC levels was also observed in primary human myoblasts at 5 days after differentiation initiation (Fig. 4J).

If ADAMTSL2 promotes myogenesis through regulation of canonical WNT signaling, then pharmacological stabilization of β-catenin with LiCl or CHIR 99021, or addition of recombinant WNT3a ligand are predicted to rescue lack of differentiation of *Adamtsl2*-KD

myoblasts [35, 36]. When *Adamtsl2*-KD myoblasts were differentiated in the presence of LiCl, CHIR 99021 or Wnt3a, we observed significant but only partial rescue of myotube formation (Fig. 5A–C). As a consequence, the fusion index was not restored to control levels, suggesting the involvement of non-canonical WNT signaling or other signaling pathways (Fig. 5D–F). To test if ADAMTSL2 required WNT ligands to regulate myoblast differentiation or if ADAMTSL2 itself could activate WNT signaling, we differentiated C2C12 myoblasts in the presence of recombinant ADAMTSL2 protein (rADAMTSL2) and the porcupine inhibitor LGK 974. Consistent with data presented in Fig. 2I–K, rADAMTSL2 protein promoted myoblast differentiation resulting in a ~1.8-fold increase in the fusion index under control conditions (Fig. 5G, H). However, LGK 974 significantly inhibited differentiation of C2C12 myoblasts in the presence of rADAMTSL2 protein. In addition, myoblasts constitutively overexpressing ADAMTSL2 did not differentiate in the presence of LGK 974 and MyHC was not induced, despite robust ADAMTSL2 overexpression (Fig. 5I). Collectively, these data indicate that ADAMTSL2 promotes myogenesis through potentiation of canonical and possibly regulation of non-canonical WNT signaling.

ADAMTSL2 binds to WNT ligands and WNT receptors

Since the data presented so far suggest that ADAMTSL2 regulates myoblast differentiation through potentiation of WNT signaling, we posited that ADAMTSL2 might directly interact with WNT ligands and/or WNT receptors. We investigated these potential interactions using co-immunoprecipitation and molecular docking experiments. When Myc-tagged ADAMTSL2 was co-expressed with the extracellular domain of the canonical WNT co-receptor LRP6, ADAMTSL2 was co-immunoprecipitated by LRP6 in the presence or absence of WNT3a ligand (Fig. 6A). When Myc-tagged ADAMTSL2 was co-expressed with V5-tagged WNT3a, ADAMTSL2 was co-immunoprecipitated by WNT3a and vice versa (Fig. 6B, C). In addition to WNT3a, Myc-tagged ADAMTSL2 was also co-immunoprecipitated by V5-tagged WNT5a (non-canonical) and V5-tagged WNT7a (canonical/non-canonical), both WNT ligands are relevant for myogenesis (Fig. 6D) [37–39]. To map the WNT-ligand binding sites in ADAMTSL2, we co-expressed Myc-tagged N- and C-terminal ADAMTSL2 domains with V5-tagged WNT3a (Fig. 6E). By co-immunoprecipitation we localized one WNT3a binding site in the TRS1-Cys domains and one in the TSR2–7 domains (Fig. 6F). Based on equal input, WNT3a binding to TSR2–7 appeared to be much stronger.

To gain further molecular insights, we used AlphaFold to model the interaction between the C-terminal TSR2–7 domains of human ADAMTSL2 and WNT3 based on their respective primary amino acid sequences. The AlphaFold model of the TSR2–7 – WNT3 complex placed the TSR2–4 domains of ADAMTSL2 adjacent to WNT3 with the greatest inter-domain interactions predicted to be with TSR3 and TSR4 (Fig. 6G). This was also reflected in the heat map of the predicted Local Distance Difference Test scores for the accuracy of the given alignment of individual TSR domains with WNT3 (Fig. 6H). To validate the AlphaFold model, we fine-mapped the WNT3a binding site in the C-terminal region of ADAMTSL2 by co-immunoprecipitation using constructs spanning the TSR2–7 domains (Fig. 6I). Consistent with the AlphaFold model, we localized the WNT3a binding site to

TSR3 since Myc-tagged TSR2–3 and TSR3–4 co-immunoprecipitated V5-tagged WNT3a equally efficiently, while TSR5–7 failed to robustly interact with WNT3a (Fig. 6J, K). However, promotion of myoblast formation required the TSR2–4 domains, which increased the fusion index by ~2-fold compared to a ~1.4-fold increase when TSR2–3 or TSR 3–4 were overexpressed (Fig. 6L, M). Together, our data show that ADAMTSL2 may promote WNT signaling by directly binding to WNT ligands and WNT receptors.

Adamtsl2 deletion in myogenic precursor cells compromises skeletal muscle architecture

To determine the role of ADAMTSL2 in vivo, we first characterized the spatiotemporal expression pattern of *Adamtsl2* in skeletal muscle. *Adamtsl2* was expressed in tibialis anterior (TA), EDL, gastrocnemius (GM) and soleus (SOL) muscles with an up to 3-fold difference between individual muscles (Fig. 7A). *Adamtsl2* declined during postnatal growth in the TA muscle consistent with a largely developmental and early postnatal role for ADAMTSL2 in other tissues (Fig. 7B) [19, 21, 40]. Immunostaining of TA and EDL muscle cross-sections showed ADAMTSL2 localization in the endomysium surrounding myofibers (Fig. 7C, Supplemental Fig. S1A, B). ADAMTSL2 staining was strong near PAX7-positive satellite cells and PDGFRα-positive fibroadipogenic progenitors (FAPs) (Fig. 7D, E). To determine, if ADAMTSL2 is required for muscle development in vivo, we inactivated *Adamtsl2* in muscle precursor cells by combining a *Myf5*-Cre allele with a previously described conditional *Adamtsl2* allele (Adamtsl2-fl/fl, Ctrl) resulting in CKO-Myf5 mice [40, 41]. *Adamtsl2* mRNA and protein were significantly reduced in 4-week old CKO-Myf5 TA muscle compared to Ctrl littermates (Fig. 7F–H). We observed increased muscle weight and myofiber cross-sectional area in CKO-Myf5 TA and EDL, but not GM muscles (Fig. 7I–K). When *Adamtsl2* was inactivated in mature myofibers using muscle-specific creatinine kinase (*Ckmm*)-Cre, muscle weight and myofiber cross-sectional area did not change, indicating that ADAMTSL2 does not play a role in mature myofibers under homeostatic conditions (Supplemental Figure S1C–E) [42]. Consistent with our in vitro data from *Adamtsl2*-KD myoblasts, differentiation of primary myoblasts from Ctrl and CKO-Myf5 EDL muscles was delayed resulting in a ~2–3-fold reduction in the fusion index at 2 and 3 days after initiation of differentiation (Fig. 7L, M). In addition, β-catenin levels were reduced in differentiating (day 2), but not proliferating (day 0) primary CKO-Myf5 myoblasts (Fig. 7N, O). These data suggest that ADAMTSL2 in myogenic-precursor cells is required for muscle development and/or postnatal growth, where it may function as a rheostat for WNT signaling or integrate WNT signaling with other signaling pathways.

Discussion

Skeletal muscle formation is regulated through dynamic interactions between muscle-resident cells and their respective microenvironments as well as through secreted niche ligands. Key players in these regulatory networks are matricellular proteins, such as ADAMTSL2, which are ECM proteins that have regulatory rather than structural roles and are characterized by highly dynamic and cell type-specific expression patterns [16]. Here, we identified an unexpected function for ADAMTSL2 in skeletal muscle as a regulator of myogenesis. Mechanistically, ADAMTSL2 promoted WNT signaling downstream of MYOD, a key myogenic transcription factor, by interacting with WNT ligands and the

canonical WNT co-receptor LRP6. Since WNT signaling induces MYOD expression and ADAMTSL2 expression is regulated by MYOD, we propose a positive feedback loop, where ADAMTSL2 augments MYOD expression through WNT signaling to accelerate or sustain myogenesis (Fig. 8).

ADAMTSL2 has previously been described as a negative regulator of TGFβ signaling [19–22]. However, we did not detect overt alterations in canonical TGFβ signaling in ADAMTSL2-deficient myoblasts. As an alternative, we considered regulation of canonical WNT signaling based on its prominent role in myoblast differentiation and skeletal muscle development and the enrichment of DEGs from *Adamtsl2*-KD myoblasts in WNT signaling-related molecular pathways [7]. Canonical WNT signaling is required for myoblast differentiation at multiple steps on their trajectory towards myotubes, including induction of MYOD [8–10, 33, 43, 44]. Since blocking secretion of all WNT ligands abolished the capacity of ADAMTSL2 to promote myoblast differentiation, we considered that its pro-myogenic function is mediated through WNT ligand-dependent signaling pathways and not through direct activation of WNT signaling by ADAMTSL2. The fact that we only partially rescued ADAMTSL2-deficiency by pharmacologic activation of canonical WNT signaling and that ADAMTSL2 can bind to several canonical and non-canonical WNT ligands suggested that ADAMTSL2 could potentially regulate both, canonical and non-canonical WNT signaling. In vivo, ADAMTSL2 may not be selective for specific WNT ligands, but modulate WNT signaling solely depending on the WNT ligands that are present in a given microenvironment. Alternatively, ADAMTSL2 could shift the balance between canonical and non-canonical WNT signaling or integrate WNT signaling with other signaling pathways, such as TGFβ signaling [45–48]. Mechanistically, ADAMTSL2 could potentiate WNT signaling by promoting the WNT ligand/WNT receptor interaction and possibly form a molecular complex with WNT ligand, LRP6, and Frizzled receptors since their WNT ligand binding sites are predicted to be accessible in our AlphaFold model [49]. As a precedent, it was shown that the ECM protein biglycan bound to WNT3a and promoted its activity by simultaneously binding to LRP6 [17]. Collectively, we propose that ADAMTSL2 regulates WNT signaling as a rheostat rather than an "on-off" switch and may affect amplitude and duration of the WNT signal. By dispatching ADAMTSL2 and other regulators, myoblasts can fine-tune WNT signaling without the need to regulate individual components of the WNT signaling pathway.

Pathogenic variants in *ADAMTSL2* cause GD in humans resulting in short stature and a pseudomuscular build characterized by apparent muscle hypertrophy [22]. In congruence, inactivation of *Adamtsl2* in MYF5-positive myogenic precursor cells in vivo resulted in increased muscle mass and myofiber cross-sectional area. This would suggest that dysfunctional or absent ADAMTSL2 enhances myogenesis or promotes muscle fiber hypertrophy. However, our gain- and loss-of-ADAMTSL2 function studies in myoblasts in vitro suggested that ADAMTSL2 promotes myogenesis and the prediction for a loss-of-function phenotype in vivo would be reduced muscle size or impaired myogenesis. How can these contrasting findings be reconciled? First, C2C12 myoblasts were derived from adult myoblasts after injury [50]. Therefore, C2C12 cells are more representative of adult skeletal muscle regeneration after injury rather than embryonic or postnatal skeletal muscle development, which differs with respect to myoblast origin and growth factor sensitivities

[12]. However, some of our findings were recapitulated in adult human myoblasts. Second, most *ADAMTSL2* variants causing GD are single nucleotide variants, which result in reduced, but not abolished ADAMTSL2 secretion [51, 52]. This would suggest that residual amounts of ADAMTSL2 are secreted in GD and a complete knockout of *Adamtsl2* may not faithfully recapitulate the consequence of GD-causing pathogenic *ADAMTSL2* variants, including potential negative consequences of accumulation of faulty ADAMTSL2 in the secretory pathway. To distinguish between consequences of lack of ADAMTSL2 in *Adamtsl2* KO mice and GD-causing *ADAMTSL2* variants, knock-in mice of pathogenic *Adamtsl2* variants are currently under investigation.

In summary, we identified a novel function for ADAMTSL2 in regulating WNT signaling during myogenesis as part of a WNT-mediated positive feedback loop that augments MYOD expression (Fig. 8). It will be exciting to elucidate further the role of ADAMTSL2 in potentially mediating tissue-specific WNT-TGFβ signaling crosstalk and to determine the role of different pools of ADAMTSL2 in skeletal muscle contributed by differentiating myogenic precursor cells and muscle connective tissue cells during skeletal muscle development and regeneration. Finally, it will be important to define the pathogenic mechanisms of GD and to examine the consequences of disease-causing variants in *ADAMTSL2*, not only in skeletal muscle, but also during development and homeostasis of other tissues affected in patients with GD, including airways, lungs, skin, and heart valves.

Experimental Procedures

Mice

B6.129S4-*Myf5*$^{tm3(cre)Sor}$/J (JAX 007893) and B6.FVB(129S4)-Tg(*Ckmm*-cre)^{5Khn}/J (JAX 006475) strains were purchased from the Jackson Laboratory (Bar Harbor, ME) [41, 42]. Mice harboring the conditional *Adamtsl2* allele were described previously [40]. Mice were used with approval from the Institutional Animal Care and Use Committee at the Icahn School of Medicine at Mount Sinai (IACUC-2018-0009, PROTO202000259). Mice were housed in a temperature-controlled environment with free access to food and water under a 12 h light/dark cycle. Mice were euthanized by CO_2 asphyxiation followed by cervical dislocation prior to tissue or cell extraction.

Cell culture

Human embryonic kidney (HEK) 293 cells (CRL-1573, ATCC) and C2C12 myoblasts (CRL-1772, ATCC) were cultured in Dulbecco's modified Eagle's medium (DMEM, GIBCO) supplemented with 10% fetal bovine serum, 1 mM sodium pyruvate (GIBCO), 100 units penicillin/100 μg/ml streptomycin (GIBCO) (complete DMEM) [50]. C2C12 myoblasts were maintained by passaging at low cell densities for up to 25 passages. Differentiation was induced by switching confluent C2C12 myoblasts to DMEM supplemented with 2% horse serum (GIBCO), 1 mM sodium pyruvate and 100 units penicillin/100 μg/ml streptomycin (differentiation medium). Primary human myoblasts were purchased from Cook MyoSite (P01606-17F.3) and cultured under proliferating conditions in MyoTonic Basal Medium (MB-2222) with MyoTonic Growth Supplement (MS-3333) per supplier's instructions. Differentiation of confluent human myoblasts was

initiated by switching to MyoTonic Differentiation Medium (MD-5555) and monitoring myotube formation by brightfield microscopy. Cultured cells were incubated in a humidified incubator in a 5% CO_2 atmosphere at 37 °C.

Isolation of primary myogenic progenitor cells (myoblasts)

EDL muscles from wild-type mice were minced and digested with 1 ml 0.2% Collagenase IV (Worthington) in DMEM with 1 mM sodium pyruvate at 37 °C for 45 min to release individual myofibers [53]. Myofibers were transferred into one well of a 6-well plate pre-coated with horse serum and incubated in DMEM with sodium pyruvate. This step was repeated twice resulting in the release of muscle progenitor cells from myofibers. Myoblasts were cultured in Ham's F12 medium (GIBCO) supplemented with 1 mM sodium pyruvate, 20% fetal bovine serum, 0.5 nM FGF-2 (Sigma Aldrich), 100 units penicillin/100 μg/ml streptomycin. Differentiation of primary myoblasts at confluency was initiated by switching to differentiation medium.

Transfection and generation of stable cell lines

Transfection of HEK 293 cells with plasmid DNA was performed with PEI reagent (Polysciences) in a 1:1 (w/w) ratio to plasmid DNA in serum-free Opti-minimal essential medium (Opti-MEM) (GIBCO). C2C12 myoblasts were transfected using TransfeX reagent (ATCC) at a ratio of 1 μg plasmid DNA to 2 μl transfection reagent according to the manufacturer's instructions. For the generation of C2C12 myoblasts stably expressing human ADAMTSL2, we used lentivirus-mediated transduction of an expression plasmid (synthesized by Vector Builder), which contained a separate green-fluorescent protein (GFP) expression cassette for fluorescence-activated cell sorting (FACS). To produce the lentivirus, HEK 293T packaging cells (3×10^6) were seeded in complete DMEM. After 24 h cells were co-transfected with 1.3 pmol of psPAX2 (Addgene, 12260), 0.72 pmol pCMV-VSV-G (Addgene, 8454) and 1.64 pmol ADAMTSL2 plasmids using PEI reagent. Supernatant containing the virus was harvested at 48, 72 and 96 h post transfection, centrifuged at 500 g for 5 min, passed through a 0.45 μm syringe filter, and stored in batches at −80 °C. To stably deplete ADAMTSL2 mRNA, C2C12 myoblasts were transfected with plasmids encoding small hairpin (sh)-RNA targeting *Adamtsl2* (Mission shRNA, Sigma Aldrich) using PEI. Stable cells were selected with 5 μg/ml puromycin (VWR) in complete DMEM for 3 days and subsequently maintained in complete DMEM plus 3 μg/ml puromycin. Knockdown efficiency of three individual shRNAs targeting different regions of the *Adamtsl2* mRNA (XM_130065.5-1977s1c1, XM_130065.5-3086s1c1, and XM_130065.5-972s1c1) was similar and we used XM_130065.5-3086s1c1 targeting the 3'-untranslated region (UTR) of *Adamtsl2*, since it does not interfere with rescue experiments using plasmids encoding recombinant ADAMTSL2. Human myoblasts were transfected using Lipofectamine LTX with Plus reagent (Invitrogen) according to the manufacturer's protocol.

Cloning of plasmids encoding recombinant ADAMTSL2 domains

Recombinant human ADAMTSL2 constructs where generated by PCR-amplification with the Q5 Hot start high fidelity 2x master mix (NEB) and specific primer pairs to allow for restriction cloning. Cloning primers are listed in Supplemental Table S1. PCR products

were amplified with the following program: 98 °C for 30 s, 34 cycles of 98 °C for 10 s, 55 °C for 30 s and 72 °C for 30 s/kb followed by a final extension for 2 min at 72 °C. The PCR products and the pSecTag 2B vector (ThermoFisher Scientific), which contains a signal peptide for secretion, were restriction-digested with BamHI × XhoI (NEB) and the agarose gel-purified DNA fragments were ligated with T4 DNA ligase (NEB) at 16 °C overnight. The N-terminal domains of ADAMTSL2, which include the endogenous signal peptide, were cloned in pcDNA3.1(-) Myc/His vector (ThermoFisher Scientific). Ligated plasmids were transformed in chemically competent *E. coli* DH5α cells (NEB, C2988J) and positive clones were identified by ampicillin resistance and verified by DNA sequencing after plasmid DNA extraction.

Immunoprecipitation

ADAMTSL2 and WNT3a, WNT5a, and WNT7a protein interaction studies were performed by co-transfecting HEK 293 cells in a 10 cm cell culture dish with 5 μg of pcDNA-WNT3a-V5, pcDNA-WNT5a-V5 or pcDNA-WNT7a-V5 (Addgene, 35927, 35930, 35933, gift from Marian Waterman) and 5 μg of plasmids encoding full length ADAMTSL2 or Myc/His-tagged ADAMTSL2 peptides [54]. For LRP6 and ADAMTSL2 protein interaction studies the LRP6-pCS2 (Addgene, 27242, gift from Xi He) was used for co-transfection [55]. Transfection was performed with PEI as described above. Transfected HEK 293 cells were switched to serum-free DMEM 24 h after transfection and cultured for an additional 2 days. Cell lysates were prepared using 1 ml RIPA lysis and extraction buffer (ThermoFisher Scientific), supplemented with cOmplete EDTA-free protease inhibitor cocktail (Roche) on ice for 30 min. Protein lysates were cleared by centrifugation at 12,000 g for 20 min at 4 °C. Protein concentrations of cell lysates were determined using a detergent-compatible Bradford assay (ThermoFisher Scientific). Co-immunoprecipitation was performed with 1 mg of protein from whole cell lysate or 4 ml of conditioned medium. Proteins binding non-specifically to protein A/G were removed by pre-adsorption of cell lysate or conditioned medium to 20 μl protein A/G magnetic beads (Pierce) for 1 h rotating at 10 rpm at 4 °C. Beads were pelleted with a magnet and protein lysates or conditioned medium were transferred into new Eppendorf tubes. 2 μg of antibodies against the V5-tag (Invitrogen, R960-25), the c-Myc tag (Invitrogen, clone 9E10, MA1–980), or LRP6 (Cell Signaling, clone C5C7, 2560) were added and incubated overnight at 4 °C under rotation. Mouse IgG (Genetex, #GTX35009) or rabbit IgG (Genetex, #GTX35035) were used as negative controls, Immunoprecipitated proteins were captured by adding 25 μl of magnetic A/G beads for 4 h at 4 °C under rotation. To remove unbound proteins, beads were pelleted and washed 3 × 5 min with 500 μl of RIPA lysis buffer under rotation at room temperature (RT). Proteins were eluted by adding 50 μl of 2x reducing SDS loading buffer, vortexing for 5 min, and incubation at 95 °C for 5 min. The eluted proteins were separated from the magnetic beads and subjected to SDS polyacrylamide gel electrophoresis (SDS-PAGE) followed by western blotting.

SDS-PAGE and western blotting

SDS-PAGE was performed with 50 μg of proteins from cell lysates or from trichloroacetic acid (TCA)-precipitated conditioned medium. For TCA precipitation, 1 ml of conditioned medium was combined with 395 μl of premixed TCA (256 μl VWR Life Science) and 1%

Triton-X 100 (139 μl, Acros Organic), vortexed for 30 sec and incubated on ice for 10 min. Precipitated proteins were pelleted by centrifugation at 10,000 rpm for 10 min at 4 °C. The protein pellet was rinsed twice with chilled acetone followed by centrifugation for 10 min at 4 °C and air dried for 5 min. The protein pellet was dissolved in 1x reducing SDS-loading buffer and incubated at 95 °C for 5 min. Proteins were resolved using SDS-PAGE and transferred onto activated polyvinylidene difluoride (PVDF) membranes (EMD Millipore) at 400 mA for 3 hours using a MiniTransblot Module (BioRad). After protein transfer, membranes were blocked for 2 h with 5% milk in PBS including 0.1% Tween-20 (PBST) at RT or overnight at 4 °C. Membranes were washed with PBST for 5 min and incubated with the following primary antibodies: GAPDH (EMD Millipore, #MAB 374, 1:2000), β-catenin (EMD Millipore, #05–613, 1:2000), LRP6 (Cell Signaling, clone C5C7, 2560), c-Myc (Invitrogen, clone 9E10, MA1–980, 1:1000), V5 (Invitrogen, #46–0705, 1:2000), ADAMTSL2 or myosin heavy chain (MyHC) (DSHB, #MF-20c, 1:1000) diluted in PBST for 2 h at RT. After washing the membranes 3×5 min with PBST, secondary antibodies goat anti-mouse (LI-COR, #IRDye 800CW/680RD) and goat anti-rabbit (LI-COR, #IRDye 680RD/800CW) at 1:10,000 dilution were added and incubated for 1 h at RT. Membranes were washed 3×5 min with PBST, 1×5 min with PBS and imaged using the Azure Biosystem c600 (Azure Biosystems). Band intensities of western blots were quantified with ImageJ. The ADAMTSL2 antibody was raised in rabbits against a peptide spanning the amino acids 552–567 of mouse ADAMTSL2 (CTHKARTRPKARKQGVS, YenZym Antibodies, LLC). The antibody was affinity purified using the immobilized immunogenic peptide.

mRNA isolation, cDNA preparation, and quantitative real-time PCR

mRNA was extracted from cell layers and skeletal muscle tissues using TRIzol (ThermoFisher Scientific). Briefly, cells were lysed in 1 ml Trizol after removing the cell culture medium and mRNA was isolated according to the manufacturer's protocol. To isolate mRNA from mouse skeletal muscle, individual muscles were dissected, snap-frozen in liquid nitrogen, and pulverized using a Geno/Grinder (Spex SamplePrep). Pulverized tissues was re-suspended in TRIzol and mRNA was isolated according to the manufacturer's protocol. After air-drying, the pellet was dissolved in nuclease-free water and mRNA concentration and purity was determined with a Nanodrop spectrophotometer (Thermo Scientific). 1 μg of mRNA was digested with DNaseI (Thermo Scientific) prior to cDNA synthesis to remove traces of genomic DNA and reverse transcribed into cDNA using the High Capacity cDNA Reverse Transcription kit (Applied Biosystem) according to the manufacturer's instructions. For quantitative real-time PCR analysis, cDNA was diluted (1:5) in nuclease-free water and a SYBR green PCR master mix (Applied Biosystem) was used to amplify gene specific PCR products with the primers listed in Supplemental Table S2. The PCR products were amplified using the following steps: 48 °C for 30 min, 95 °C for 10 min and 40 cycles of 95 °C for 15 s and 60 °C for 1 min. Cycle threshold (ct) values were used to calculate fold changes using the $2^{-(\Delta\Delta CT)}$ method and graphs were plotted using Origin 2019 (OriginLab).

RNA sequencing

sh-Ctrl and *Adamtsl2*-KD C2C12 myoblasts (3×10^5/well) were seeded in triplicates in 6-well plates and cultured in complete DMEM until confluency. To induce differentiation, C2C12 myoblasts were cultured in differentiation medium for an additional 3 days with daily medium change. After 3 days, cells were lysed with 1 ml Trizol and mRNA was extracted according to the manufacturer's protocol. RNA quality control, library preparation, sequencing and bioinformatics determination of DEGs was performed by Azenta Life sciences (Genewiz). mRNA quality was controlled using NanoDrop, RNA Qubit and Tape Station instruments. Sequencing libraries were prepared by polyA selection for mRNA and sequenced to a depth of 20–30 Mio reads (HiSeq 4000 2×150 paired-end configuration, Illumina). Sequence reads were trimmed to remove possible adapter sequences and nucleotides with poor quality using Trimmomatic v.0.36. The trimmed reads were mapped to the *Mus musculus* GRCm38 reference genome (ENSEMBL) using STAR aligner v.2.5.2b. Unique gene hit counts were calculated by using featureCounts from the Subread package v.1.5.2. Only unique reads that fell within exon regions were counted. Gene hit counts were used for downstream differential expression analysis. Using DESeq2, a comparison of gene expression between the two groups of samples was performed. The Wald test was used to generate p-values and $\log_2$-fold changes. Genes with an adjusted p-value <0.05 and absolute $\log_2$-fold change >1 were called as differentially expressed genes for each comparison. Data are available through the GEO database (GSE185894)

Immunofluorescence staining of cells

For immunofluorescence staining of proliferating and differentiating C2C12 myoblasts, 50,000 cells per chamber were seeded in 8-well glass chamber slides and cultured in complete DMEM until confluency. Differentiation was initiated by switching to differentiation medium. At the end of the culture period, cells were rinsed three times with PBS and fixed with ice-cold methanol (Fisher Chemicals) for 15 min at –20 °C. After three washes with PBS, cells were blocked with 5 % BSA in PBST for 2 h at RT. Cells were incubated with antibodies against β-catenin (EMD Millipore, # 05–613), Ki67 (Abcam, #ab16667), MyHC (DSHB, #MF 20), laminin (Sigma, #L9393 and Novus Bio, #NB600-883) or ADAMTSL2 diluted at 1:200 in PBS overnight at 4 °C. Cells were then washed 3×5 min with PBS and incubated with fluorophore-tagged goat-anti mouse or goat-anti rabbit secondary antibodies (Jackson Immuno Research, #Rhodamine Red 111-295-144 or 115-295-146 and Alexa Fluor 488 115-545-146 or 111-545-144) diluted at 1:500 in PBST for 1 h at RT. After washing 3×5 min with PBS, cells were mounted with DAPI containing mounting medium (Invitrogen) and observed using an Axio Imager Z1 fluorescence microscope (Zeiss).

Immunofluorescence staining of muscle tissue

EDL, TA and GM muscles were dissected and partially embedded in a plastic cassette holder using 1 g/ml of tragacanth powder gum (Alfa Aesar) in water. Muscles where then immersed in liquid nitrogen-chilled 2-methylbutane (Fisher Chemicals) for 2 min. Subsequently, the fixed tissues were kept in liquid nitrogen for 1 min, wrapped in aluminum foil, and stored at –80 °C. To prepare frozen sections, muscle tissues were embedded with

optimal cutting temperature (OCT) medium (Tissue-Tek) and kept at −20 °C. 20 μm sections were obtained using a cryostat (Avantik) and mounted onto frosted glass slide. Sections were incubated with 4% PFA (MP) for 20 min at RT and washed 2×10 min with PBS. The tissue was permeabilized with chilled methanol for 6 min at −20 °C and washed for 10 min with PBS. 0.01 M citric acid (Fisher BioReagents) solution in water was heated by microwaving until the temperature reached 90 °C. Sections were immersed in the hot citric acid buffer and steamed for 5 min in the microwave with 10 s on and 50 s off. Sections were cooled down in citric acid for 30 min at RT and washed for 15 min with PBS. Sections were incubated with 5 % BSA in PBS for 2 h followed by incubation in primary antibodies against laminin (LAM-89, NB600–883, Novus Biologicals), ADAMTSL2, MyHC, PAX7 (DSHB), PDGFRα (Invitrogen, #14-1401-82) were diluted 1:200 in PBS for overnight at 4 °C. Sections were washed 3×10 min with PBS and incubated with corresponding fluorophore-tagged secondary antibodies at 1:500 dilution for 1 h at RT. Slides were washed 3×10 min with PBS and mounted with DAPI-containing mounting medium and imaged.

Prediction of the ADAMTSL2-WNT complex using AlphaFold

For the generation of the ADAMTSL2 TSR2–7-WNT3 model, AlphaFold multimer models were generated using a locally installed version of AlphaFold v2.1.1 on the Computationally Shared Facility at University of Manchester [56]. The installation included the full genetic databases for multiple sequence alignments. Sequences of ADAMTSL2 (Q86TH1: 564–951) and WNT3 (P56703-1:42-355) were used for modelling. FASTA files containing complexes of the TSR domains of ADAMTSL2 and WNT3 were prepared and submitted to the AlphaFold pipeline and ranked by the software. Models were visualized in UCSF ChimeraX [57].

Statistical Analysis

Two sample comparisons were done with a two-sample Student's t-test and multi-sample comparisons with a one-way ANOVA followed by posthoc Tukey analysis to determine which samples were different. A p-value cutoff of <0.05 was considered significant. Sample sizes are indicated in the figure legends. OriginPro software was used for statistical calculations and plotting.

Supplementary Material

Refer to Web version on PubMed Central for supplementary material.

Acknowledgments:

Data Availability:

RNA sequencing data were deposited in the GEO database (GSE185894). All other data are included in the article or in supplemental materials.

References

[1]. Janssen I, Heymsfield SB, Wang ZM, and Ross R, Skeletal muscle mass and distribution in 468 men and women aged 18–88 yr, J Appl Physiol (1985) 89 (2000) 81–8. 10.1152/jappl.2000.89.1.81. [PubMed: 10904038]

[2]. Petrany MJ, and Millay DP, Cell Fusion: Merging Membranes and Making Muscle, Trends in cell biology 29 (2019) 964–973. 10.1016/j.tcb.2019.09.002. [PubMed: 31648852]

[3]. Zammit PS, Function of the myogenic regulatory factors Myf5, MyoD, Myogenin and MRF4 in skeletal muscle, satellite cells and regenerative myogenesis, Seminars in cell & developmental biology 72 (2017) 19–32. 10.1016/j.semcdb.2017.11.011. [PubMed: 29127046]

[4]. Guo K, Wang J, Andres V, Smith RC, and Walsh K, MyoD-induced expression of p21 inhibits cyclin-dependent kinase activity upon myocyte terminal differentiation, Mol. Cell. Biol 15 (1995) 3823–9. 10.1128/MCB.15.7.3823. [PubMed: 7791789]

[5]. Sabourin LA, Girgis-Gabardo A, Seale P, Asakura A, and Rudnicki MA, Reduced differentiation potential of primary MyoD−/− myogenic cells derived from adult skeletal muscle, J. Cell Biol 144 (1999) 631–43. 10.1083/jcb.144.4.631. [PubMed: 10037786]

[6]. Megeney LA, Kablar B, Garrett K, Anderson JE, and Rudnicki MA, MyoD is required for myogenic stem cell function in adult skeletal muscle, Genes Dev 10 (1996) 1173–83. 10.1101/gad.10.10.1173. [PubMed: 8675005]

[7]. Girardi F, and Le Grand F, Wnt Signaling in Skeletal Muscle Development and Regeneration, Prog Mol Biol Transl Sci 153 (2018) 157–179. 10.1016/bs.pmbts.2017.11.026. [PubMed: 29389515]

[8]. Tajbakhsh S, Borello U, Vivarelli E, Kelly R, Papkoff J, Duprez D, Buckingham M, and Cossu G, Differential activation of Myf5 and MyoD by different Wnts in explants of mouse paraxial mesoderm and the later activation of myogenesis in the absence of Myf5, Development 125 (1998) 4155–62. 10.1242/dev.125.21.4155. [PubMed: 9753670]

[9]. Suzuki A, Pelikan RC, and Iwata J, WNT/beta-Catenin Signaling Regulates Multiple Steps of Myogenesis by Regulating Step-Specific Targets, Mol. Cell. Biol 35 (2015) 1763–76. 10.1128/MCB.01180-14. [PubMed: 25755281]

[10]. Cossu G, and Borello U, Wnt signaling and the activation of myogenesis in mammals, EMBO J 18 (1999) 6867–72. 10.1093/emboj/18.24.6867. [PubMed: 10601008]

[11]. Linker C, Lesbros C, Gros J, Burrus LW, Rawls A, and Marcelle C, beta-Catenin-dependent Wnt signalling controls the epithelial organisation of somites through the activation of paraxis, Development 132 (2005) 3895–905. 10.1242/dev.01961. [PubMed: 16100089]

[12]. Hutcheson DA, Zhao J, Merrell A, Haldar M, and Kardon G, Embryonic and fetal limb myogenic cells are derived from developmentally distinct progenitors and have different requirements for beta-catenin, Genes Dev 23 (2009) 997–1013. 10.1101/gad.1769009. [PubMed: 19346403]

[13]. Brunelli S, Relaix F, Baesso S, Buckingham M, and Cossu G, Beta catenin-independent activation of MyoD in presomitic mesoderm requires PKC and depends on Pax3 transcriptional activity, Dev. Biol 304 (2007) 604–14. 10.1016/j.ydbio.2007.01.006. [PubMed: 17275805]

[14]. Gros J, Serralbo O, and Marcelle C, WNT11 acts as a directional cue to organize the elongation of early muscle fibres, Nature 457 (2009) 589–93. 10.1038/nature07564. [PubMed: 18987628]

[15]. Lukjanenko L, Karaz S, Stuelsatz P, Gurriaran-Rodriguez U, Michaud J, Dammone G, Sizzano F, Mashinchian O, Ancel S, Migliavacca E, Liot S, Jacot G, Metairon S, Raymond F, Descombes P, Palini A, Chazaud B, Rudnicki MA, Bentzinger CF, and Feige JN, Aging Disrupts Muscle Stem Cell Function by Impairing Matricellular WISP1 Secretion from Fibro-Adipogenic Progenitors, Cell Stem Cell 24 (2019) 433–446 e7. 10.1016/j.stem.2018.12.014. [PubMed: 30686765]

[16]. Murphy-Ullrich JE, and Sage EH, Revisiting the matricellular concept, Matrix Biol 37 (2014) 1–14. 10.1016/j.matbio.2014.07.005. [PubMed: 25064829]

[17]. Berendsen AD, Fisher LW, Kilts TM, Owens RT, Robey PG, Gutkind JS, and Young MF, Modulation of canonical Wnt signaling by the extracellular matrix component biglycan, Proc Natl Acad Sci U S A 108 (2011) 17022–7. 10.1073/pnas.1110629108. [PubMed: 21969569]

[18]. Robertson IB, and Rifkin DB, Regulation of the Bioavailability of TGF-beta and TGF-beta-Related Proteins, Cold Spring Harbor perspectives in biology 8 (2016) 10.1101/cshperspect.a021907.

[19]. Hubmacher D, Wang LW, Mecham RP, Reinhardt DP, and Apte SS, Adamtsl2 deletion results in bronchial fibrillin microfibril accumulation and bronchial epithelial dysplasia--a novel mouse model providing insights into geleophysic dysplasia, Dis Model Mech 8 (2015) 487–99. 10.1242/dmm.017046. [PubMed: 25762570]

[20]. Rypdal KB, Erusappan PM, Melleby AO, Seifert DE, Palmero S, Strand ME, Tonnessen T, Dahl CP, Almaas V, Hubmacher D, Apte SS, Christensen G, and Lunde IG, The extracellular matrix glycoprotein ADAMTSL2 is increased in heart failure and inhibits TGFbeta signalling in cardiac fibroblasts, Sci Rep 11 (2021) 19757. 10.1038/s41598-021-99032-2. [PubMed: 34611183]

[21]. Delhon L, Mahaut C, Goudin N, Gaudas E, Piquand K, Le Goff W, Cormier-Daire V, and Le Goff C, Impairment of chondrogenesis and microfibrillar network in Adamtsl2 deficiency, FASEB J 33 (2019) 2707–2718. 10.1096/fj.201800753RR. [PubMed: 30303737]

[22]. Le Goff C, Morice-Picard F, Dagoneau N, Wang LW, Perrot C, Crow YJ, Bauer F, Flori E, Prost-Squarcioni C, Krakow D, Ge G, Greenspan DS, Bonnet D, Le Merrer M, Munnich A, Apte SS, and Cormier-Daire V, ADAMTSL2 mutations in geleophysic dysplasia demonstrate a role for ADAMTS-like proteins in TGF-beta bioavailability regulation, Nat. Genet 40 (2008) 1119–23. 10.1038/ng.199. [PubMed: 18677313]

[23]. Koo BH, Le Goff C, Jungers KA, Vasanji A, O'Flaherty J, Weyman CM, and Apte SS, ADAMTS-like 2 (ADAMTSL2) is a secreted glycoprotein that is widely expressed during mouse embryogenesis and is regulated during skeletal myogenesis, Matrix Biol 26 (2007) 431–41. 10.1016/j.matbio.2007.03.003. [PubMed: 17509843]

[24]. Marzin P, Thierry B, Dancasius A, Cavau A, Michot C, Rondeau S, Baujat G, Phan G, Bonniere M, Le Bourgeois M, Khraiche D, Pejin Z, Bonnet D, Delacourt C, and Cormier-Daire V, Geleophysic and acromicric dysplasias: natural history, genotype-phenotype correlations, and management guidelines from 38 cases, Genet Med (2020) 10.1038/s41436-020-00994-x.

[25]. Batkovskyte D, McKenzie F, Taylan F, Simsek-Kiper PO, Nikkel SM, Ohashi H, Stevenson RE, Ha T, Cavalcanti DP, Miyahara H, Skinner SA, Aguirre MA, Akcoren Z, Utine GE, Chiu T, Shimizu K, Hammarsjo A, Boduroglu K, Moore HW, Louie RJ, Arts P, Merrihew AN, Babic M, Jackson MR, Papadogiannakis N, Lindstrand A, Nordgren A, Barnett CP, Scott HS, Chagin AS, Nishimura G, and Grigelioniene G, Al-Gazali Skeletal Dysplasia Constitutes the Lethal End of ADAMTSL2-Related Disorders, J. Bone Miner. Res (2023) 10.1002/jbmr.4799.

[26]. Steinle J, Hossain WA, Lovell S, Veatch OJ, and Butler MG, ADAMTSL2 gene variant in patients with features of autosomal dominant connective tissue disorders, American journal of medical genetics Part A 185 (2021) 743–752. 10.1002/ajmg.a.62030. [PubMed: 33369194]

[27]. Lagord C, Soulet L, Bonavaud S, Bassaglia Y, Rey C, Barlovatz-Meimon G, Gautron J, and Martelly I, Differential myogenicity of satellite cells isolated from extensor digitorum longus (EDL) and soleus rat muscles revealed in vitro, Cell Tissue Res 291 (1998) 455–68. 10.1007/s004410051015. [PubMed: 9477302]

[28]. Zhao Y, Zhou J, He L, Li Y, Yuan J, Sun K, Chen X, Bao X, Esteban MA, Sun H, and Wang H, MyoD induced enhancer RNA interacts with hnRNPL to activate target gene transcription during myogenic differentiation, Nat Commun 10 (2019) 5787. 10.1038/s41467-019-13598-0. [PubMed: 31857580]

[29]. Liu J, Pan S, Hsieh MH, Ng N, Sun F, Wang T, Kasibhatla S, Schuller AG, Li AG, Cheng D, Li J, Tompkins C, Pferdekamper A, Steffy A, Cheng J, Kowal C, Phung V, Guo G, Wang Y, Graham MP, Flynn S, Brenner JC, Li C, Villarroel MC, Schultz PG, Wu X, McNamara P, Sellers WR, Petruzzelli L, Boral AL, Seidel HM, McLaughlin ME, Che J, Carey TE, Vanasse G, and Harris JL, Targeting Wnt-driven cancer through the inhibition of Porcupine by LGK974, Proc Natl Acad Sci U S A 110 (2013) 20224–9. 10.1073/pnas.1314239110. [PubMed: 24277854]

[30]. Massague J, Cheifetz S, Endo T, and Nadal-Ginard B, Type beta transforming growth factor is an inhibitor of myogenic differentiation, Proc Natl Acad Sci U S A 83 (1986) 8206–10. 10.1073/pnas.83.21.8206. [PubMed: 3022285]

[31]. Liu D, Black BL, and Derynck R, TGF-beta inhibits muscle differentiation through functional repression of myogenic transcription factors by Smad3, Genes Dev 15 (2001) 2950–66. 10.1101/gad.925901. [PubMed: 11711431]

[32]. Li J, Wang Y, Wang Y, Yan Y, Tong H, and Li S, Fibronectin type III domain containing four promotes differentiation of C2C12 through the Wnt/beta-catenin signaling pathway, FASEB J 34 (2020) 7759–7772. 10.1096/fj.201902860RRR. [PubMed: 32298013]

[33]. Tanaka S, Terada K, and Nohno T, Canonical Wnt signaling is involved in switching from cell proliferation to myogenic differentiation of mouse myoblast cells, J Mol Signal 6 (2011) 12. 10.1186/1750-2187-6-12. [PubMed: 21970630]

[34]. Hedgepeth CM, Conrad LJ, Zhang J, Huang HC, Lee VM, and Klein PS, Activation of the Wnt signaling pathway: a molecular mechanism for lithium action, Dev. Biol 185 (1997) 82–91. 10.1006/dbio.1997.8552. [PubMed: 9169052]

[35]. Ring DB, Johnson KW, Henriksen EJ, Nuss JM, Goff D, Kinnick TR, Ma ST, Reeder JW, Samuels I, Slabiak T, Wagman AS, Hammond ME, and Harrison SD, Selective glycogen synthase kinase 3 inhibitors potentiate insulin activation of glucose transport and utilization in vitro and in vivo, Diabetes 52 (2003) 588–95. 10.2337/diabetes.52.3.588. [PubMed: 12606497]

[36]. Clement-Lacroix P, Ai M, Morvan F, Roman-Roman S, Vayssiere B, Belleville C, Estrera K, Warman ML, Baron R, and Rawadi G, Lrp5-independent activation of Wnt signaling by lithium chloride increases bone formation and bone mass in mice, Proc Natl Acad Sci U S A 102 (2005) 17406–11. 10.1073/pnas.0505259102. [PubMed: 16293698]

[37]. von Maltzahn J, Bentzinger CF, and Rudnicki MA, Wnt7a-Fzd7 signalling directly activates the Akt/mTOR anabolic growth pathway in skeletal muscle, Nat. Cell Biol 14 (2011) 186–91. 10.1038/ncb2404. [PubMed: 22179044]

[38]. Le Grand F, Jones AE, Seale V, Scime A, and Rudnicki MA, Wnt7a activates the planar cell polarity pathway to drive the symmetric expansion of satellite stem cells, Cell Stem Cell 4 (2009) 535–47. 10.1016/j.stem.2009.03.013. [PubMed: 19497282]

[39]. Reggio A, Rosina M, Palma A, Cerquone Perpetuini A, Petrilli LL, Gargioli C, Fuoco C, Micarelli E, Giuliani G, Cerretani M, Bresciani A, Sacco F, Castagnoli L, and Cesareni G, Adipogenesis of skeletal muscle fibro/adipogenic progenitors is affected by the WNT5a/GSK3/beta-catenin axis, Cell Death Differ 27 (2020) 2921–2941. 10.1038/s41418-020-0551-y. [PubMed: 32382110]

[40]. Hubmacher D, Taye N, Balic Z, Thacker S, Adams SM, Birk DE, Schweitzer R, and Apte SS, Limb- and tendon-specific Adamtsl2 deletion identifies a role for ADAMTSL2 in tendon growth in a mouse model for geleophysic dysplasia, Matrix Biol 82 (2019) 38–53. 10.1016/j.matbio.2019.02.001. [PubMed: 30738849]

[41]. Tallquist MD, Weismann KE, Hellstrom M, and Soriano P, Early myotome specification regulates PDGFA expression and axial skeleton development, Development 127 (2000) 5059–70. 10.1242/dev.127.23.5059. [PubMed: 11060232]

[42]. Bruning JC, Michael MD, Winnay JN, Hayashi T, Horsch D, Accili D, Goodyear LJ, and Kahn CR, A muscle-specific insulin receptor knockout exhibits features of the metabolic syndrome of NIDDM without altering glucose tolerance, Mol. Cell 2 (1998) 559–69. 10.1016/s1097-2765(00)80155-0. [PubMed: 9844629]

[43]. Brack AS, Conboy IM, Conboy MJ, Shen J, and Rando TA, A temporal switch from notch to Wnt signaling in muscle stem cells is necessary for normal adult myogenesis, Cell Stem Cell 2 (2008) 50–9. 10.1016/j.stem.2007.10.006. [PubMed: 18371421]

[44]. Cui S, Li L, Yu RT, Downes M, Evans RM, Hulin JA, Makarenkova HP, and Meech R, beta-Catenin is essential for differentiation of primary myoblasts via cooperation with MyoD and alpha-catenin, Development 146 (2019) 10.1242/dev.167080.

[45]. Contreras O, Soliman H, Theret M, Rossi FMV, and Brandan E, TGF-beta-driven downregulation of the transcription factor TCF7L2 affects Wnt/beta-catenin signaling in PDGFRalpha(+) fibroblasts, J. Cell Sci 133 (2020) 10.1242/jcs.242297.

[46]. Dzialo E, Tkacz K, and Blyszczuk P, Crosstalk between the TGF-beta and WNT signalling pathways during cardiac fibrogenesis, Acta Biochim. Pol 65 (2018) 341–349. 10.18388/abp.2018_2635. [PubMed: 30040870]

[47]. Biressi S, Miyabara EH, Gopinath SD, Carlig PM, and Rando TA, A Wnt-TGFbeta2 axis induces a fibrogenic program in muscle stem cells from dystrophic mice, Sci Transl Med 6 (2014) 267ra176. 10.1126/scitranslmed.3008411.

[48]. Carthy JM, Garmaroudi FS, Luo Z, and McManus BM, Wnt3a induces myofibroblast differentiation by upregulating TGF-beta signaling through SMAD2 in a beta-catenin-dependent manner, PloS one 6 (2011) e19809. 10.1371/journal.pone.0019809. [PubMed: 21611174]

[49]. Hirai H, Matoba K, Mihara E, Arimori T, and Takagi J, Crystal structure of a mammalian Wnt-frizzled complex, Nat Struct Mol Biol 26 (2019) 372–379. 10.1038/s41594-019-0216-z. [PubMed: 31036956]

[50]. Yaffe D, and Saxel O, Serial passaging and differentiation of myogenic cells isolated from dystrophic mouse muscle, Nature 270 (1977) 725–7. 10.1038/270725a0. [PubMed: 563524]

[51]. Piccolo P, Sabatino V, Mithbaokar P, Polishchuck E, Law SK, Magraner-Pardo L, Pons T, Polishchuck R, and Brunetti-Pierri N, Geleophysic dysplasia: novel missense variants and insights into ADAMTSL2 intracellular trafficking, Mol Genet Metab Rep 21 (2019) 100504. 10.1016/j.ymgmr.2019.100504. [PubMed: 31516831]

[52]. Bader HL, Ruhe AL, Wang LW, Wong AK, Walsh KF, Packer RA, Mitelman J, Robertson KR, O'Brien DP, Broman KW, Shelton GD, Apte SS, and Neff MW, An ADAMTSL2 founder mutation causes Musladin-Lueke Syndrome, a heritable disorder of beagle dogs, featuring stiff skin and joint contractures, PloS one 5 (2010) e12817. 10.1371/journal.pone.0012817. [PubMed: 20862248]

[53]. Pasut A, Jones AE, and Rudnicki MA, Isolation and culture of individual myofibers and their satellite cells from adult skeletal muscle, J Vis Exp (2013) e50074. 10.3791/50074. [PubMed: 23542587]

[54]. Najdi R, Proffitt K, Sprowl S, Kaur S, Yu J, Covey TM, Virshup DM, and Waterman ML, A uniform human Wnt expression library reveals a shared secretory pathway and unique signaling activities, Differentiation 84 (2012) 203–13. 10.1016/j.diff.2012.06.004. [PubMed: 22784633]

[55]. Tamai K, Semenov M, Kato Y, Spokony R, Liu C, Katsuyama Y, Hess F, Saint-Jeannet JP, and He X, LDL-receptor-related proteins in Wnt signal transduction, Nature 407 (2000) 530–5. 10.1038/35035117. [PubMed: 11029007]

[56]. Jumper J, Evans R, Pritzel A, Green T, Figurnov M, Ronneberger O, Tunyasuvunakool K, Bates R, Zidek A, Potapenko A, Bridgland A, Meyer C, Kohl SAA, Ballard AJ, Cowie A, Romera-Paredes B, Nikolov S, Jain R, Adler J, Back T, Petersen S, Reiman D, Clancy E, Zielinski M, Steinegger M, Pacholska M, Berghammer T, Bodenstein S, Silver D, Vinyals O, Senior AW, Kavukcuoglu K, Kohli P, and Hassabis D, Highly accurate protein structure prediction with AlphaFold, Nature 596 (2021) 583–589. 10.1038/s41586-021-03819-2. [PubMed: 34265844]

[57]. Pettersen EF, Goddard TD, Huang CC, Meng EC, Couch GS, Croll TI, Morris JH, and Ferrin TE, UCSF ChimeraX: Structure visualization for researchers, educators, and developers, Protein Sci 30 (2021) 70–82. 10.1002/pro.3943. [PubMed: 32881101]

Highlights:

- ADAMTS-like 2 regulates MYOD through a WNT-driven positive feedback loop during myogenesis.

- ADAMTS-like 2 potentiates WNT signaling by binding to WNT ligands through its TSR2–4 domains and WNT receptors.

- ADAMTS-like 2 deficiency in myogenic progenitor cells causes aberrant skeletal muscle development.
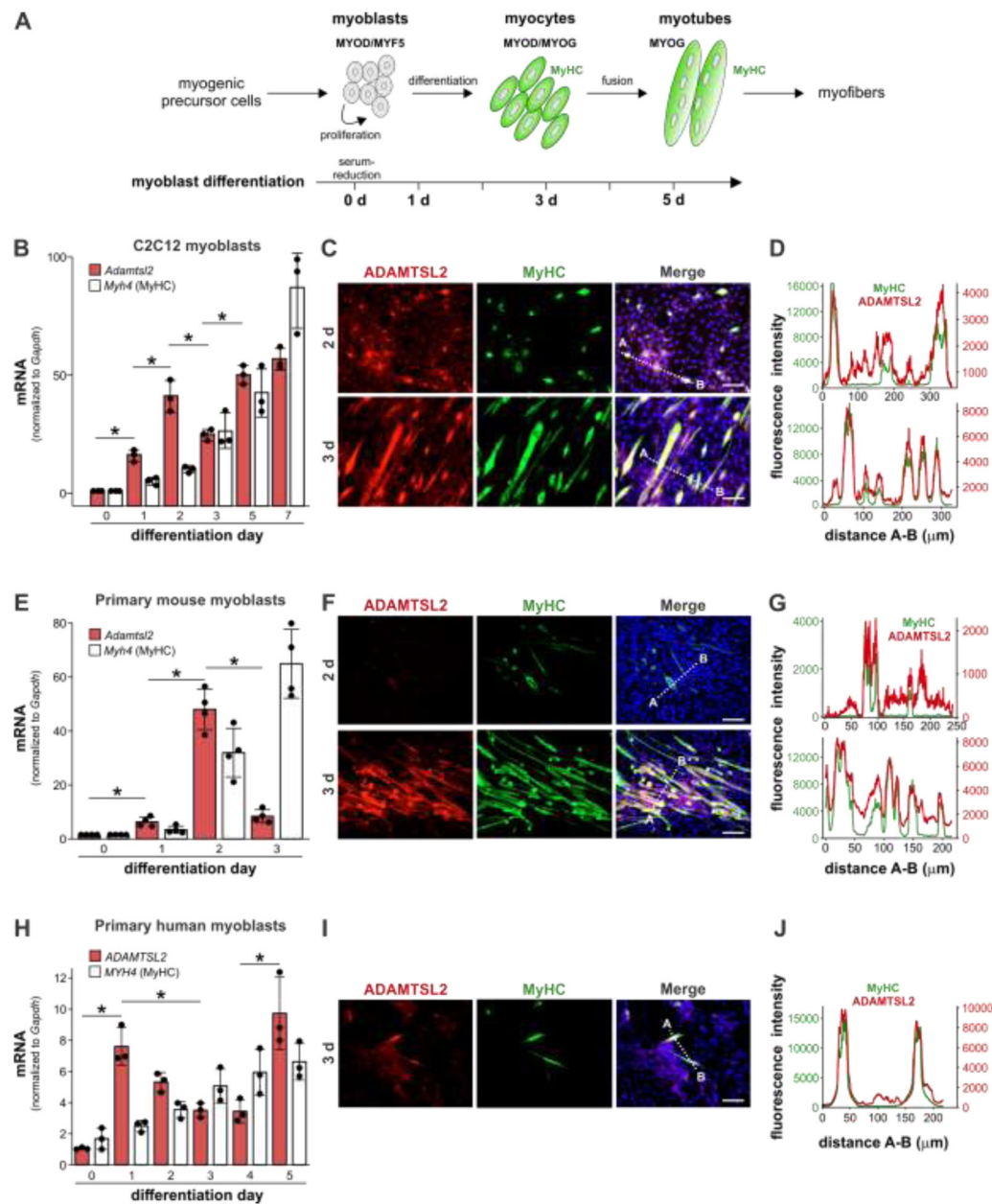
Figure 1.
ADAMTSL2 is expressed during myoblast differentiation. (*A*) Diagram of myogenesis. Key stages of myoblast differentiation and associated myogenic regulatory factors are bolded. The approximate timeline of myoblast differentiation after serum reduction in vitro is indicated. MyHC, myosin heavy chain (gene: *MYH4*). (*B*) Normalized ADAMTSL2 and MYH4 mRNA levels in differentiating C2C12 myoblasts undergoing differentiation by serum reduction (n = 3). Increasing MYH4 mRNA levels indicate differentiation towards myotubes. (*C*) ADAMTSL2 and MyHC immunostaining of C2C12 myoblasts at day 2 and 3 after differentiation initiation. (*D*) Fluorescence intensity blots of green (MyHC) and red (ADAMTSL2) channels along the lines indicated in C. (*E*) Normalized ADAMTSL2 and MYH4 mRNA levels in differentiating primary mouse myoblasts from wild-type EDL

muscle (n = 4). Increasing MYH4 mRNA levels indicate differentiation towards myotubes. (*F*) ADAMTSL2 and myosin heavy chain (MyHC) immunostaining of primary myoblasts at day 2 and 3 after differentiation initiation. (*G*) Fluorescence intensity blots of green (MyHC) and red (ADAMTSL2) channels along the lines indicated in F. (*H*) Normalized ADAMTSL2 and MYH4 mRNA levels in differentiating primary human myoblasts (n = 3). Increasing MYH4 mRNA levels indicate differentiation towards myotubes. (*I*) ADAMTSL2 and myosin heavy chain (MyHC) immunostaining of primary human myoblasts at day 3 after differentiation initiation. (*J*) Fluorescence intensity blots of green (MyHC) and red (ADAMTSL2) channels along the lines indicated in I. mRNA levels in B, E, H were normalized to *Gapdh* and day 0 was set as 1. Bars represent mean ±SD. P-values were determined by one-way ANOVA and posthoc Tukey test. $*p < 0.05$. Scale bars: 100 μm.
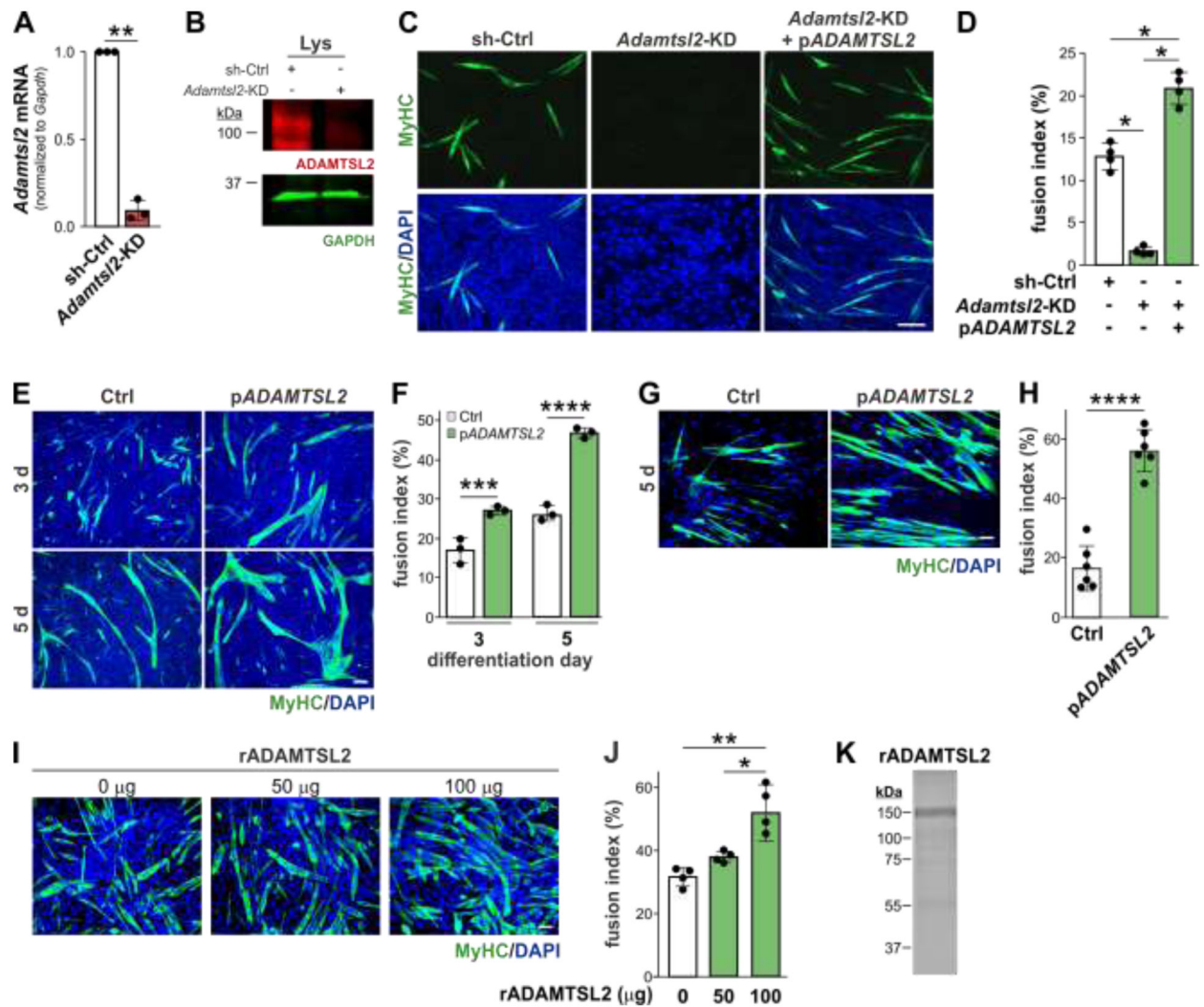
Figure 2.
ADAMTSL2 is required for myoblast differentiation. (*A*) Normalized ADAMTSL2 mRNA levels in proliferating C2C12 myoblasts after stable knock-down of ADAMTSL2 with shRNA (*Adamtsl2*-KD) compared to controls (sh-Ctrl) expressing non-targeting shRNA (n = 3). (*B*) Western blot analysis of ADAMTSL2 in myoblast lysates (Lys) from *Adamtsl2*-KD and sh-Ctrl cells. (*C*) MyHC immunostaining of sh-Ctrl and *Adamtsl2*-KD myoblasts at day 3 after differentiation initiation and rescue of myotube formation by transient overexpression of ADAMTSL2 (p*ADAMTSL2*). (*D*) Quantification of fusion index from C (n = 4). (*E*) MyHC immunostaining of vector control (Ctrl) or *ADAMTSL2* overexpressing C2C12 myoblasts at day 3 and 5 after differentiation initiation. (*F*) Quantification of fusion index from E (n = 3). (*G*) MyHC immunostaining of vector control (Ctrl) or *ADAMTSL2* overexpressing primary human myoblasts at day 5 after differentiation initiation. (*H*) Quantification of fusion index from G (n = 3, 2 fields of view). (*I*) MyHC immunostaining of C2C12 myoblasts differentiated for 3 days in the presence of 0 (PBS), 50 or 100 μg recombinant ADAMTSL2 protein (rADAMTSL2). (*J*) Quantification of fusion index from I (n = 4). (*K*) Coomassie brilliant blue staining of 5 μg recombinant ADAMTSL2 protein
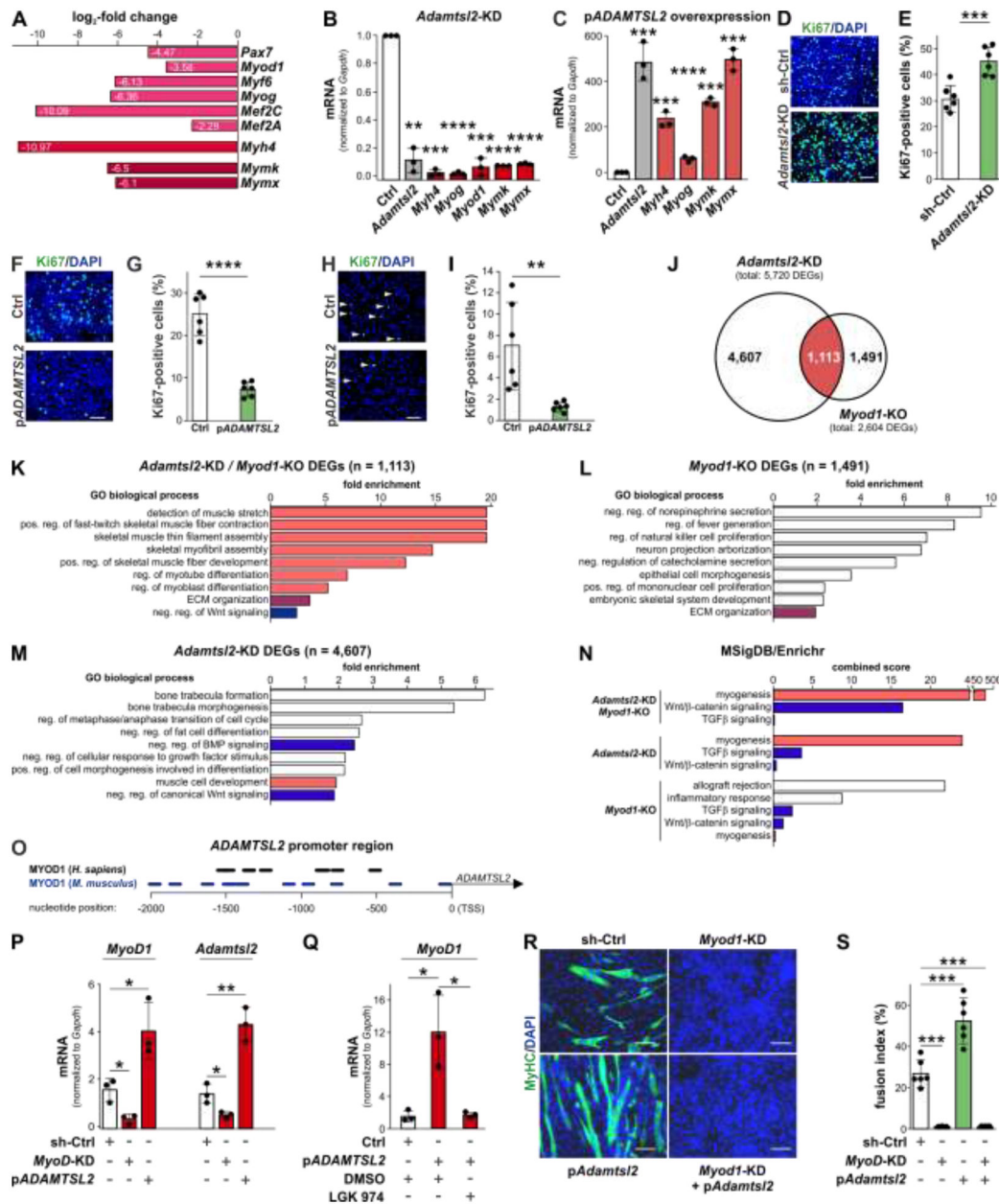
after SDS-PAGE. Bars in A, D, F, H, J represent mean ±SD. P-values were determined by Student's t-test (A, F, H) or one-way ANOVA and posthoc Tukey test (D, J). *p<0.05, **p<0.01, ***p<0.001, ****p<0.0001. Scale bars: 100 μm.
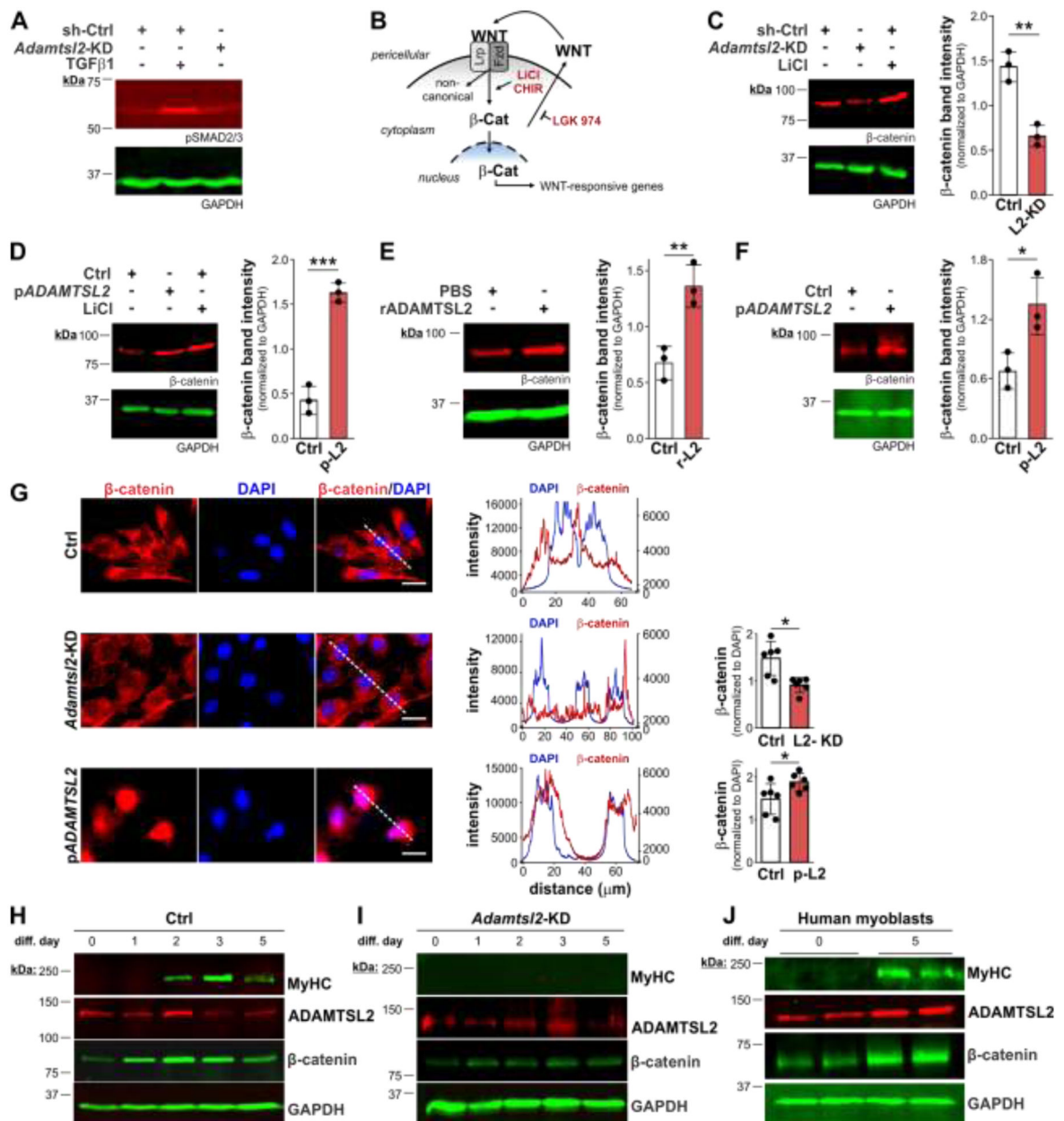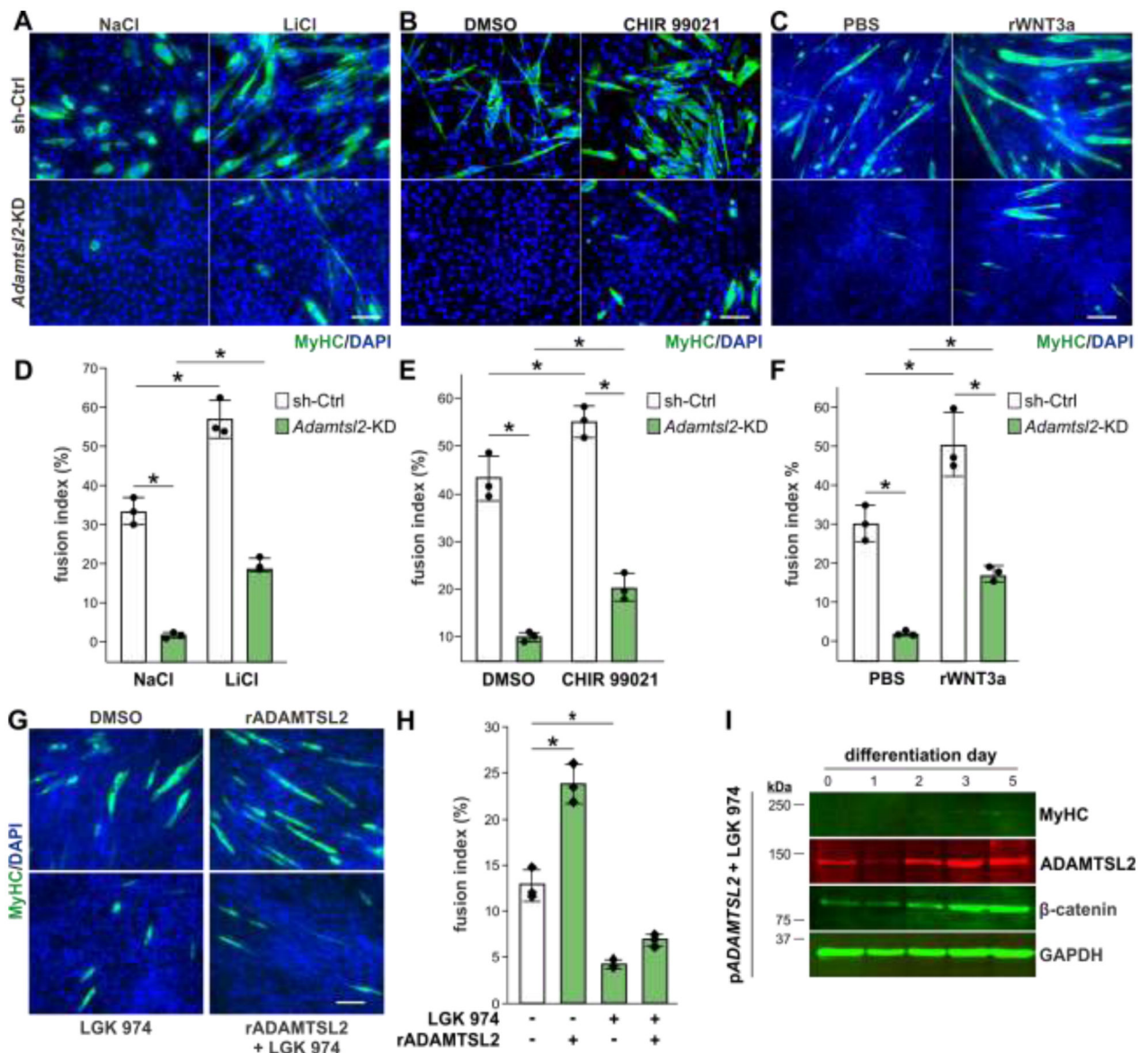
Figure 3.
ADAMTSL2 promotes myoblast differentiation downstream of MYOD. (*A*) Log$_2$-fold
change of selected differentially expressed genes (DEGs) of *Adamtsl2*-KD compared to
sh-Ctrl C2C12 myoblasts at 3 days after differentiation initiation identified by RNAseq
(n=3). (*B*) Validation of DEGs from A in independent biological replicates by qRT-PCR
in *Adamtsl2*-KD and sh-Ctrl C2C12 myoblasts at 3 days after differentiation initiation (n
= 3). (*C*) Normalized mRNA levels in p*ADAMTSL2*-overexpressing C2C12 myoblasts at
3 days after differentiation initiation (n = 3). (*D, E*) Ki67 immunostaining of proliferating
C2C12 myoblasts (D) and quantification of Ki67-positive cells (E) in sh-Ctrl and *Adamtsl2-*
KD cells 3 days after differentiation initiation (n = 4). (*F, G*) Ki67 immunostaining of
proliferating C2C12 myoblasts (F) and quantification of Ki67-positive cells (G) in Ctrl and

p*ADAMTSL2*-overexpressing cells 3 days after differentiation initiation (n = 4). (*H, I*) Ki67 immunostaining of proliferating primary human myoblasts (H) and quantification of Ki67-positive cells (I) in Ctrl and p*ADAMTSL2*-overexpressing cells 3 days after differentiation initiation (n = 4). (*J*) Venn diagram of DEGs shared between *Adamtsl2*-KD and *Myod1*-KO. (*K-M*) Gene Ontology (GO) biological processes enriched in shared DEGs (K), *Myod1*-KO only DEGs (L) and *Adamtsl2*-KD only DEGs (M). (*N*) Molecular Signature Database (MSigDB) processes enriched in *Adamtsl2*-KD/*Myod1*-KO shared and distinct DEGs. (*O*) Localization of putative MYOD recognition sequences in mouse and human ADAMTSL2 promoter regions. TSS, transcriptional start site. (*P*) Normalized MYOD and ADAMTSL2 mRNA levels after *Myod1*-KD or *Adamtsl2* overexpression compared to sh-Ctrl C2C12 myoblasts (n=3). (*Q*) Normalized MYOD mRNA levels after overexpression of *Adamtsl2* in the presence or absence of the porcupine inhibitor LGK 974 (n=3). *(R)* MyHC-positive myotubes of sh-Ctrl and *Myod1*-KD myoblasts with and without overexpression of p*ADAMTSL2* at 3 days after initiation of differentiation. (*S*) Quantification of fusion index from R (n = 3, 2–3 images per fields-of-view). Bars in B, C, E, G, I, P, Q, S represent mean values ±SD. P-values were determined by Student's t-test (B, C, E, G, I) or one-way ANOVA and posthoc Tukey test (P, Q, S). *p<0.05, **p<0.01, ***p<0.001, ****p<0.0001. Scale bars in D, F, H, R: 100 μm.
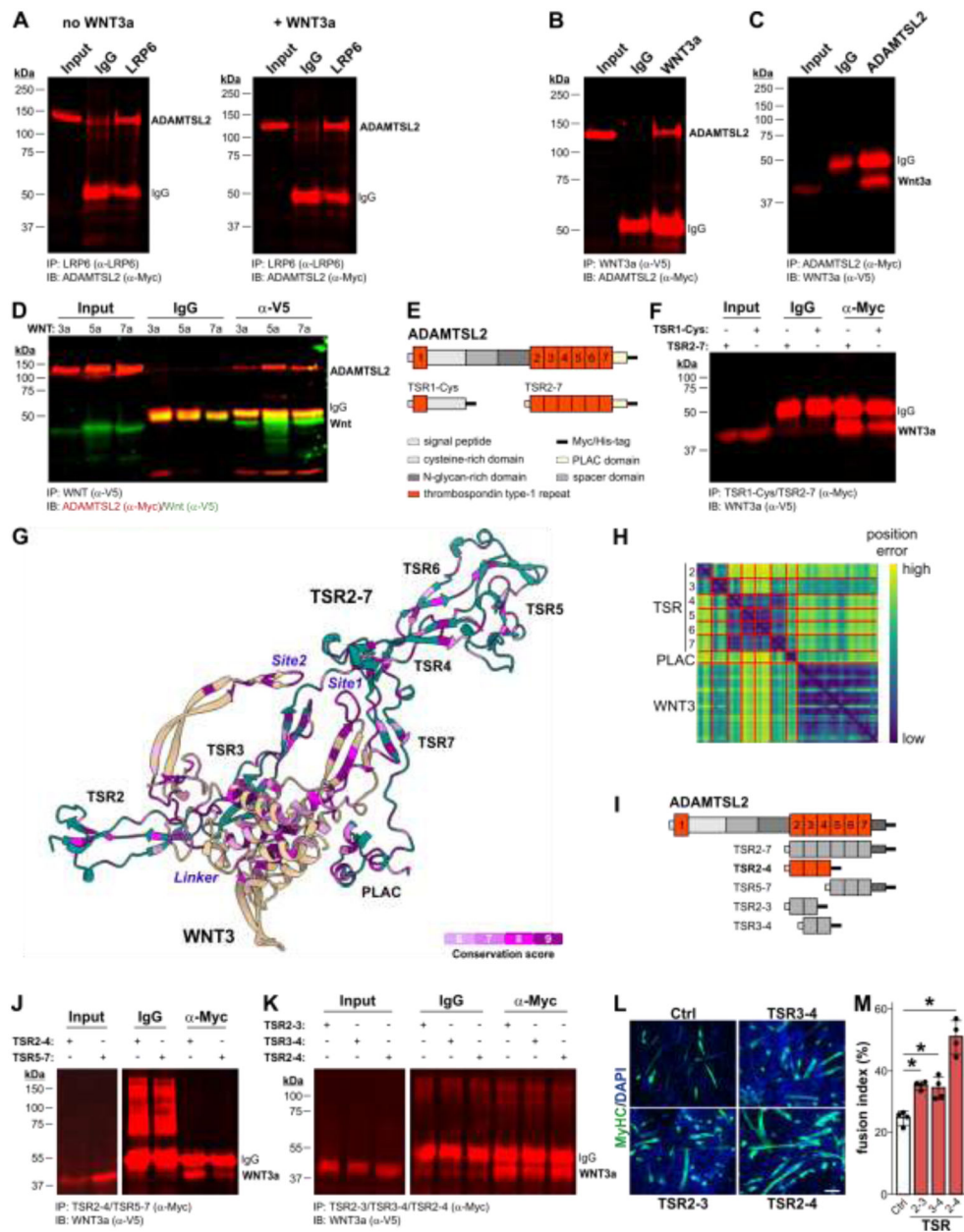
Figure 4.
ADAMTSL2 promotes canonical WNT/β-catenin signaling. (*A*) Western blot analysis of
SMAD2/3 phosphorylation in lysates from sh-Ctrl and *Adamtsl2-KD* C2C12 myoblasts
under proliferating conditions. Addition of 10 ng/ml recombinant TGFβ1 was used as
positive control. (*B*) Schematic of canonical WNT signaling and targets of activators
(CHIR, LiCl) and inhibitors (LGK 974). β-Cat, β-catenin. (*C*) Western blot analysis and
quantification of β-catenin in sh-Ctrl and *Adamtsl2-KD* C2C12 myoblast lysates under
proliferating conditions (n=3). (*D*) Western blot analysis and quantification of β-catenin
in Ctrl and p*ADAMTSL2* overexpressing C2C12 myoblast lysates under proliferating
conditions (n=3). LiCl was used as positive control in C and D. (*E*) Western blot
analysis and quantification of β-catenin in C2C12 myoblast lysates treated with 100

µg/ml ADAMTSL2 protein (rADAMTSL2) under proliferating conditions. (*F*) Western blot analysis and quantification of β-catenin in Ctrl and p*ADAMTSL2* overexpressing primary human myoblast lysates under proliferating conditions. In C, D, E, F β-catenin band intensities were normalized to GAPDH as a loading control and quantified from n=3 blots. (*G*) β-catenin immunostaining (left), intensity profiles along lines indicated in the merged image (middle), and quantification of the β-catenin signal (right) in proliferating Ctrl, *Adamtsl2-KD* and p*ADAMTSL2* overexpressing C2C12 myoblasts (n=3, 2 fields of view). (*H, I*) Western blot analysis of ADAMTSL2, MyHC, and β-catenin in sh-Ctrl (H) and *Adamtsl2-KD* (I) C2C12 myoblast lysates during differentiation. (*J*) Western blot analysis of ADAMTSL2, MyHC, and β-catenin in primary human myoblast lysates at 0 and 5 days after differentiation initiation. Scale bars: 20 µm. Bars in C-G represent mean values ±SD and p-values were calculated with a two-sided Student's t-test. *p<0.05, **p<0.01, ***p<0.001.

Figure 5.
Activation of canonical WNT signaling partially rescues ADAMTSL2 deficiency. (*A-C*)
MyHC immunostaining of sh-Ctrl and *Adamtsl2-KD* C2C12 myoblasts treated with 10
mM LiCl (A), 5 μM CHIR 99021 (B) or 100 ng/ml recombinant WNT3a (rWNT3a) (C).
(*D-F*) Quantification of fusion indices from A-C (n = 3). (*G*) MyHC immunostaining of
C2C12 myoblasts differentiated in the presence of 100 μg recombinant ADAMTSL2 and the
porcupine inhibitor LGK 974 at 3 days after differentiation initiation. (*H*) Quantification of
fusion index from N (n=3). (*I*) Western blot analysis of ADAMTSL2, MyHC, and β-catenin
in differentiating p*ADAMTSL2* overexpressing C2C12 myoblast lysates after treatment with
LGK 974. Scale bars: 20 μm (F), 100 μm in H-J. Bars represent mean ±SD. P-values were
determined by one-way ANOVA and posthoc Tukey test. *p<0.05.

Figure 6.
ADAMTSL2 binds to WNT ligands and WNT receptors. (*A*) Western blot analysis of ADAMTSL2 co-immunoprecipitated by LRP6 without (left) or with (right) WNT3a overexpression. (*B*) Western blot analysis of ADAMTSL2 co-immunoprecipitated by WNT3a. (*C*) Western blot analysis of WNT3a co-immunoprecipitated by ADAMTSL2. (*D*) Western blot analysis of ADAMTSL2 co-immunoprecipitated by WNT3a, WNT5a or WNT7a. (*E*) Domain organization of ADAMTSL2 showing TSR1-Cys and TSR2–7 constructs. (*F*) Western blot analysis of WNT3a co-immunoprecipitated by TSR1-Cys and TSR2–7. (G) AlphaFold modeling and prediction of WNT3 interactions with TSR2–7 domains of ADAMTSL2. Site 1 and 2 of WNT3 mediate the interaction with frizzled receptors and the WNT3 linker region mediates the interaction with LRP6. (*H*) Heat map

of predicted local distance difference test (pLDDT) scores for G. (*I*) Domain organization of C-terminal ADAMTSL2 constructs. (*J*) Western blot of WNT3a co-immunoprecipitated by TSR2–4 or TSR5–7. (*K*) Western blot of WNT3a co-immunoprecipitated by TSR2–3, TSR3–4 or TSR2–4. (*L*) MyHC staining of C2C12 myoblasts transiently transfected with empty vector or plasmids encoding TSR2–3, TSR3–4 and TSR2–4 3 days after differentiation initiation. Scale bars: 100 μm. (*M*) Quantification of fusion index from (L) (n = 3). Bars represent mean ±SD. P-values were determined by one-way ANOVA and post-hoc Tukey test. *p<0.05. IP, immunoprecipitation; IB, immunoblot.
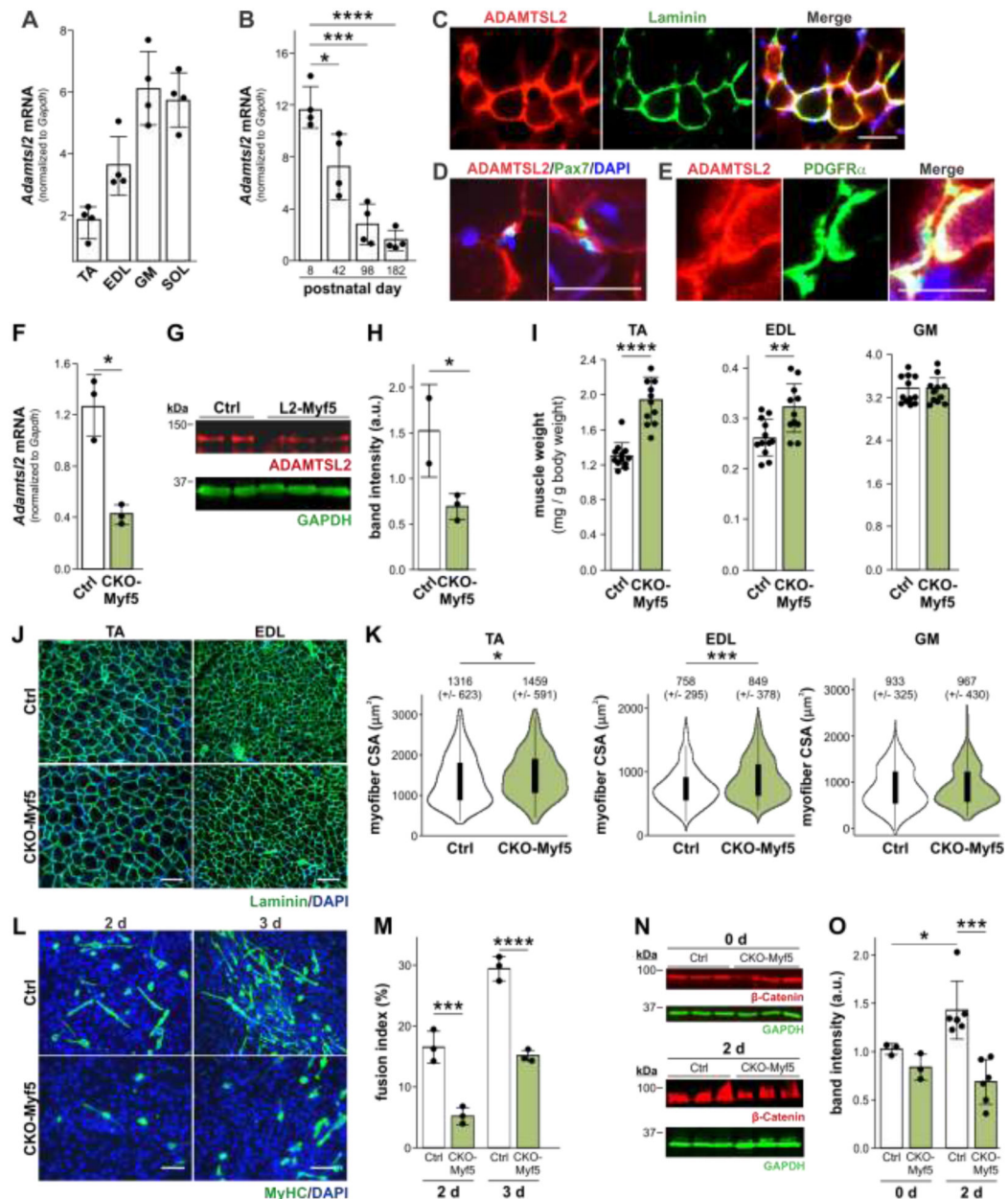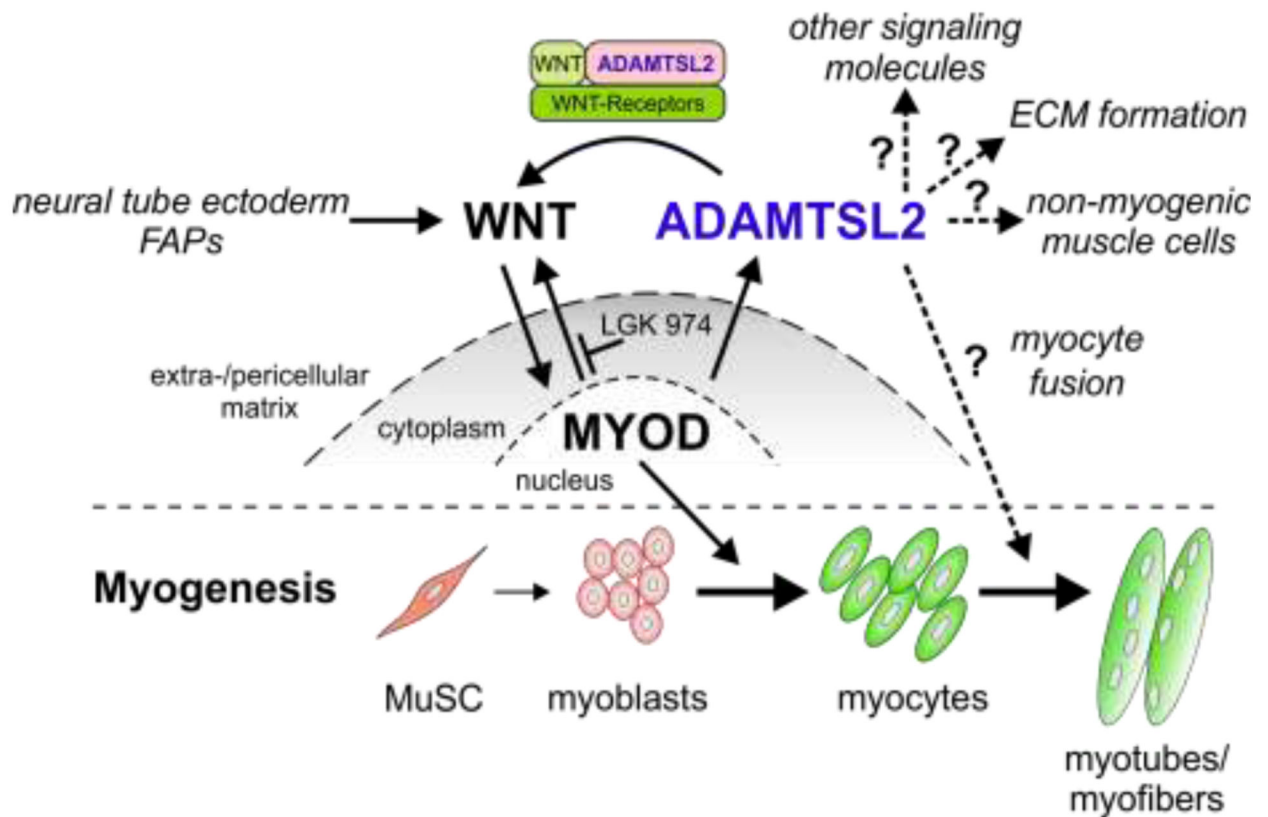
Figure 7.
ADAMTSL2-depletion in *Myf5*-positive myogenic progenitor cells alters skeletal muscle
architecture. (*A*) Normalized *Adamtsl2* mRNA levels in 4-week-old wild-type tibialis
anterior (TA), extensor digitorum longus (EDL), gastrocnemius (GM) and soleus (SOL)
muscle (n = 4). (*B*) Normalized *Adamtsl2* mRNA levels in wild-type TA muscle during
postnatal growth (n = 4). (*C*) ADAMTSL2 and laminin immunostaining of wild-type
TA cross-sections. (*D*) ADAMTSL2 and PAX7 immunostaining of wild-type TA cross-
sections. (*E*) ADAMTSL2 and PDGFRα immunostaining of wild-type TA cross-sections.
(*F*) *Adamtsl2* expression in TA muscle after *Myf5*-Cre-mediated *Adamtsl2* ablation (CKO-
Myf5) compared to Ctrl (n = 3). (*G*) Western blot analysis of ADAMTSL2 in extracts from
Ctrl and CKO-Myf5 EDL muscle. GAPDH was used as loading control. (*H*) Quantification

of band intensity in B normalized to GAPDH. (*I*) TA, EDL and GM muscle weight from 8-week-old CKO-Myf5 and Ctrl mice normalized to body weight (n = 11). (*J*) Laminin immunostaining of TA and EDL cross sections from 4-week-old CKO-Myf5 and Ctrl mice. (*K*) Violin plots of myofiber cross-sectional area from J (n = 3). Boxes represent 25th-75th percentile, whiskers ±SD. Mean values (μm^2) ±SD are indicated above the violin plots. (*L*) MyHC immunostaining of primary CKO-Myf5 and Ctrl EDL-derived myoblasts at day 2 and 3 after initiation of differentiation. (*M*) Quantification of fusion index from (L) (n = 3). (*N*) Western blot analysis of β-catenin in protein extracts from Ctrl and CKO-Myf5 primary myoblasts. GAPDH was used as loading control. (*O*) Quantification of band intensity from N normalized to GAPDH (n=3 for 0 d, n=6 for 2 d). Bars in A, B, F, H, I, M. O represent mean ±SD. P-values were determined with a Student's t-test. *p<0.05, **p<0.01, ***p<0.001, ****p<0.0001. Scale bars in C, D, E: 50 μm; in J, L: 100 μm.

Figure 8.
Proposed model for the pro-myogenic function of ADAMTSL2 in skeletal muscle. To initiate the formation of myotubes, MYOD is induced by WNT ligands secreted from the dorsal neural tube and dorsal ectoderm during development or from fibroadipogenic progenitors (FAPs) during skeletal muscle regeneration after injury. MYOD induces ADAMTSL2 expression, which in turn augments canonical and/or non-canonical WNT signaling by promoting WNT ligand/WNT receptor interactions and further augments or sustains MYOD levels. This positive feedback loop results in augmentation of myogenesis. If ADAMTSL2 promotes myocyte fusion, acts on other non-myogenic skeletal muscle cell types, or correlates multiple signaling pathways needs further investigation.